UNIVERSIDADE FEDERAL DE ALFENAS

JOÃO FRANCISCO VITÓRIO RODRIGUES

TRANSCRIPTOMA INTEGRATIVO DE CÉLULAS HUMANAS TRATADAS COM DIFERENTES TIPOS DE NANOPARTÍCULAS

Alfenas/MG

2021

JOÃO FRANCISCO VITÓRIO RODRIGUES

TRANSCRIPTOMA INTEGRATIVO DE CÉLULAS HUMANAS TRATADAS COM DIFERENTES TIPOS DE NANOPARTÍCULAS

Dissertação apresentada como parte dos requisitos para obtenção do título de Mestre em Ciências Biológicas pela Universidade Federal de Alfenas.

Área de concentração: Interação Patógeno-Hospedeiro.

Orientador: Prof. Dr. Luiz Felipe Leomil Coelho

Alfenas/MG

2021

Dados Internacionais de Catalogação-na-Publicação (CIP)
Sistema de Bibliotecas da Universidade Federal de Alfenas
Biblioteca Central – Campus Sede

Rodrigues, João Francisco Vitório
R696t Transcriptoma integrativo de células humanas tratadas com diferentes tipos de nanopartículas / João Francisco Vitório Rodrigues – Alfenas, MG, 2021.
68 f.: il. –

Orientador: Luiz Felipe Leomil Coelho.
Dissertação (Mestrado em Ciências Biológicas) – Universidade Federal de Alfenas, 2021.
Bibliografia.

1. Nanopartículas. 2. Transcriptoma. 3. Expressão gênica. I. Coelho, Luiz Felipe Leomil. II. Título.

CDD- 575

Ficha Catalográfica elaborada por Marlom Cesar da Silva
Bibliotecário-Documentalista CRB6/2735

JOÃO FRANCISCO VITÓRIO RODRIGUES

TRANSCRIPTOMA INTEGRATIVO DE CÉLULAS HUMANAS TRATADAS COM DIFERENTES TIPOS DE NANOPARTÍCULAS

A Banca examinadora abaixo-assinada aprova a Dissertação apresentada como parte dos requisitos para a obtenção do título de Mestre em Ciências Biológicas pela Universidade Federal de Alfenas. Área de concentração: Interação Patógeno-Hospedeiro.

Aprovada em: 23 de fevereiro de 2021.

Prof. Dr. Luiz Felipe Leomil Coelho
Instituição: Universidade Federal de Alfenas - UNIFAL-MG

Profa. Dra. Anna Carolina Toledo da Cunha Pereira
Instituição: Universidade Federal do Delta do Parnaíba

Profa. Dra. Eva Burger
Instituição: Universidade Federal de Alfenas - UNIFAL-MG

Documento assinado eletronicamente por **Luiz Felipe Leomil Coelho**, **Professor do Magistério Superior**, em 23/02/2021, às 10:08, conforme horário oficial de Brasília, com fundamento no art. 6º, § 1º, do Decreto nº 8.539, de 8 de outubro de 2015.

Documento assinado eletronicamente por **Eva Burger**, **Professor do Magistério Superior**, em 23/02/2021, às 10:11, conforme horário oficial de Brasília, com fundamento no art. 6º, § 1º, do Decreto nº 8.539, de 8 de outubro de 2015.

Documento assinado eletronicamente por **Anna Carolina Toledo da Cunha Pereira**, **Usuário Externo**, em 23/02/2021, às 10:12, conforme horário oficial de Brasília, com fundamento no art. 6º, § 1º, do Decreto nº 8.539, de 8 de outubro de 2015.

A autenticidade deste documento pode ser conferida no site https://sei.unifal-mg.edu.br/sei/controlador_externo.php?acao=documento_conferir&id_orgao_acesso_externo=0, informando o código verificador **0468919** e o código CRC **48DF554C**.

Dedico esse trabalho aos meus pais Marcos e Rosangela que foram a raiz de minhas realizações, minha esposa Cristiane minha fonte de sustentação e amor e a meus filhos Kaique e Elisa os saborosos frutos da minha existência.

AGRADECIMENTO

Agradeço, primeiramente, a meu orientador Luiz Felipe Leomil Coelho, pela paciência, dedicação, apoio e liberdade para realizar o trabalho.

A minha família que sempre esteve lá em meus altos e baixos.

E, não menos importante, a Deus detentor de todo poder, honra e glória.

O presente trabalho foi realizado com apoio da Coordenação de Aperfeiçoamento de Pessoal de Nível Superior - Brasil (CAPES) - Código de Financiamento 001.

RESUMO

Nanopartículas (NPs) são partículas que possuem tamanho inferior a 100 nM. As NPs podem ser produzidas de diversos materiais orgânicos e inorgânicos e em diversas formas (por exemplo nanotubos, nanoesferas e nanobastões). Esta tecnologia apresenta potencial promissor para várias aplicações biológicas tendo em vista a sua possibilidade de funcionalização, o que permite o seu direcionamento seletivo para órgãos, tecidos e células. A aplicabilidade na saúde humana está relacionada ao uso das NPs como estimuladores do sistema imune quando conjugados com antígenos, no uso para o diagnóstico e tratamento de tumores e para a entrega de medicamentos em determinados tecidos e órgãos. Apesar do uso das NPs em novos sistemas de diagnóstico, tratamento ou prevenção para doenças humanas, poucos estudos são realizados para verificar o efeito das NPs sobre o transcriptoma celular. A análise integrativa de transcriptoma (ITA) é atualmente reconhecida como uma técnica promissora para a compreensão de eventos biológicos a partir da análise de diversos transcriptomas depositados em bancos de dados públicos. Essa abordagem permite não só avaliar quais genes são diferentemente expressos nas diversas condições, mas também é capaz de inferir sobre suas as respectivas vias biológicas ativadas após um determinado estímulo. Nessa pesquisa foram identificados 81 transcriptomas derivados de células humanas tratadas com NPs no banco de dados Gene Expression Omnibus (GEO). Destes, 45 foram selecionados por serem transcriptomas de células tratadas com NPs compostas apenas de um material (sem associação ou conjugação com nenhuma outra substância ou material) e células não tratadas. Os demais foram excluídos por terem dados incompletos, não terem sido realizados em duplicatas, falta de grupo controle, e por serem de dados derivados de células tratadas com NPs composta por mais de um material. Assim sendo, devido a variabilidade desses estudos, somente foram selecionados transcriptomas de células tratadas com NPs por 24 horas. Dessa forma, foram utilizados 30 conjuntos de dados que compreendem transcriptomas derivados de 5 materiais e 6 células diferentes. A ITA utilizou os genes diferencialmente expressos (DEGs) identificados em cada um dos transcriptomas e demonstrou que existe uma especificidade na resposta celular aos diferentes tipos de NPs. Poucos DEGs apresentaram expressão em comum à dois ou mais transcriptomas analisados. A análise de vias biológicas apresentou uma diversidade de vias ativadas e suprimidas pelos diferentes tratamentos com poucas vias compartilhadas entre os diferentes transcriptomas analisados. Portanto, a ITA de células humanas tratadas com diferentes tipos de NPs demonstra uma resposta transcricional específica e dependente do tipo de material utilizado na nanopartícula e do tipo celular.

Palavras-chave: Nanopartícula. Transcriptoma integrativo. Genes diferencialmente expressos.

ABSTRACT

Nanoparticles (NPs) are defined as a particle of matter that is between 1 and 100 nanometers (nm) in at least one side. NPs can be produced from different organic and inorganic materials and in different forms (example: nanotubes, nanospheres and nanorods). This technology has a promising potential for several biological applications due to its possibility of functionalization which allows the selective delivery of nanoparticles to organs, tissues, and cells. The applicability in human health is related to the use of NPs as stimulators of the immune system when they are conjugated with antigens, in the diagnosis and treatment of tumors, and also as delivery drugs systems to target organs and tissues. Despite the use of NPs in new diagnostic, treatment, and prevention technologies for human diseases, few studies are conducted to verify the effect of NPs on the cellular transcriptome. Integrative transcriptome analysis (ITA) is currently recognized as a promising technique for understanding biological events through the analysis of several transcriptomes deposited in public databases. This approach allows not only evaluating which genes are expressed differently in different conditions but also can infer the biological pathways activated after a specific stimulus. In this research, 81 transcriptomes derived from human cells treated with nanoparticles were identified in the Gene Expression Omnibus (GEO) database. Of these, 45 were selected because they are transcriptomes of cells treated with nanoparticles composed only of one material (without association or conjugation with any other substance or material) and untreated cells. The other studies were excluded due to lack of data, absence of replicates, absence of control group, and because they are derived from cells treated with nanoparticles composed of more than one material. Therefore, due to the variability of these studies, only transcriptomes of cells treated with NPs for 24 hours were selected. Thus, 30 datasets were used and these comprising transcriptomes derived from 5 materials and 6 different cells. ITA used the differentially expressed genes (DEGs) in each of the transcriptomes and demonstrated a specificity in the cellular response to different types of NPs. Few DEGs were common on two or more analyzed transcriptomes. The analysis of biological pathways showed a high diversity of biological pathways that were activated or suppressed by the different treatments and also a very low number of shared pathways among the transcriptomes. Therefore, the ITA of human cell transcriptomes treated with different nanoparticles demonstrates a specific transcriptional response to material and also to the cell type.

Keywords: Nanoparticle. Integrative transcriptome. Differentially expressed genes.

LISTA DE FIGURAS

LISTA DE TABELAS

LISTA DE ABREVIATURAS E SIGLAS

16LU	Human fibroblastos
ITA	Integrative Transcriptome Analysis
CACO2	Human colon adenocarcinoma
CSV	Comma-separated values
DEGs	Genes differentially expressed
GEO	Gene Expression Omnibus
HANPs	Hydroxyapatite nanoparticle
HCC-LM3	Human liver carcinoma
HDF	Human Dermal Fibroblast
HEPG2	Human liver carcinoma
HET1A	Human esophageal epithelial
HUVEC	Human umbilical vein endothelial cell
JURKAT	Human T lymphocyte leukemia
KEGG	Kyoto Encyclopedia of Genes and Genomes
MCF7	Human breast adenocarcinoma
nm	Nanometers
NPs	Nanoparticles
PAMAM	Polyamidoamine dendrimer
PBAE447	β-amino esters 447
PC3	Human prostatic adenocarcinoma
PLGA	Poly-lactic-co-glycolic acid
PMMAEA	Ethyl acrylate-co-methyl methacrylate-co-trimethylammonioethyl methacrylate chloride
PST-DOX	Galactoxyloglucan polysaccharide
RNAseq	RNA sequencing
SAE	Human small airway epithelial cells
THP1	Human macrophages

SUMÁRIO

1 INTRODUÇÃO GERAL

Atualmente o diagnóstico e tratamento de doenças humanas encontram barreiras que dificultam a sua eficácia. A não especificidade de fármacos, os efeitos colaterais adversos e a dificuldade na obtenção de imagens são algumas dificuldades presentes na medicina. Assim sendo, a busca de novas tecnologias que podem contribuir para a melhora desse cenário é imprescindível. (CHAKRABORTY; RAHMAN, 2012; ZUGAZAGOITIA *et al.*, 2016; MANSON *et al.*, 2020).

A Nanotecnologia se apresenta como uma ferramenta valiosa para vencer essas barreiras através do desenvolvimento de NPs. Dotadas de um tamanho peculiar as NPs variam entre 1 e 100 nanômetros (nm) em pelo menos uma de suas dimensões externas. Além do tamanho diminuto, as NPs possuem propriedades diferentes dos materiais de origem em sua forma macro (WOLFRAM *et al*., 2016). Tais propriedades permitem que as NPs possam ser submetidas ao processo de funcionalização. Esse pode, por exemplo, direcionar a ação das NPs em células alvo ou ainda facilitar o transporte de fármaco nos diferentes tecidos do organismo (BOUCHOUCHA *et al.*, 2016; LI *et al.*, 2016). As NPs podem ser usadas para o tratamento de câncer reduzindo os efeitos colaterais dos fármacos e entregando o tratamento exclusivamente para células cancerígenas (TABASUM *et al.*, 2017). As NPs podem ser usadas como contraste em diagnósticos por imagem, como parte de formulações vacinais (ADAIR, 2009; SULCZEWSKI *et al.*, 2018), como bloqueadoras de raio UV (OSMOND; MCCALL, 2010) ou como desinfetantes de superfície (RAI; YADAV; GADE, 2009).

As NPs podem ser encontradas naturalmente no meio ambiente ou produzidas em laboratório e podem ser produzidas com um ou mais materiais. Os materiais mais comumente utilizados são metais, lipídios, polímeros, silíca, proteínas e carbono. As NPs podem apresentar diferentes morfologias, tais como nanoconchas, nanobastões, lipossomas, dendrímeros, esferas, discos, cilindros, cones, tubos e fios (VENTOLA; BHARALI; MOUSA, 2010). A carga da NPs e o seu tamanho também podem variar facilitando ou não a endocitose/fagocitose (GRZINCIC *et al.*, 2015). As propriedades magnéticas, óticas, mecânicas e térmicas diferenciais das NPs também representam uma vantagem para o seu uso (KHAN; SAEED; KHAN, 2019). Assim, a partir do uso da nanotecnologia na medicina surgiu um novo campo de estudo a nanomedicina (PAUTLER; BRENNER, 2010).

Apesar da nanomedicina ser uma área promissora, existe uma deficiência na condução de estudos para embasar o uso seguro das NPs (KUNZMANN *et al*., 2011; MAYNARD, 2012). A interação célula-nanoparticula, sua biodistribuição, bioacumulação, mecanismos de citotoxicidade e decomposição são questões pouco elucidadas uma vez que uma pequena variação na composição, tamanho, morfologia, etc. podem desencadear respostas celulares diferentes (GRZINCIC *et al.*, 2015). Avaliar cada resposta

as suas variações em modelos *in vivo* não é uma opção viável dada à quantidade de animais, às questões éticas, o tempo e ao dinheiro que seriam dispendidos realizando os protocolos experimentais (KOOTER *et al*., 2019). Assim sendo, protocolos experimentais *in vitro* devem ser amplamente utilizados de forma que os estudos sejam conduzidos simultaneamente com quantidade menor de NPs, reagentes e células tornando o trabalho mais rápido e barato e sem esbarrar nas questões éticas (WANG, LIYING *et al.*, 2014).

O transcriptoma é uma das opções existentes para avaliar os protocolos experimentais realizados *in vitro* e *in vivo,* uma vez que é capaz de analisar a resposta celular em nível molecular. Esta metodologia pode analisar todos os transcritos de uma célula revelando detalhes do processo de regulação gênica em determinadas situações ou estímulos. Duas técnicas se destacam atualmente no estudo do transcriptoma, o microarranjo de DNA (microarray) e o seqüenciamento de RNA (RNAseq). O microarray apresenta a limitação de apenas trabalhar com organismos padrões e com o monitoramento da expressão dos genes que estão presentes no microarranjo. Já o RNAseq por sua vez, possui a capacidade de analisar de forma global os genes diferencialmente expressos de qualquer organismo apresentando assim uma versatilidade que o torna mais atrativo (WANG, ZHONG; GERSTEIN; SNYDER, 2009). Cada transcriptoma analisado gera um conjunto de dados (*dataset*) que representam o conjunto de todos os transcritos quantificados através dessas técnicas. Os dataset são depositados em bancos públicos como o Gene Expression Omnibus (https://www.ncbi.nlm.nih.gov/geo/) e ficam disponíveis para análises por outros grupos de pesquisadores. A análise integrativa de transcriptoma (ITA) é atualmente reconhecida como uma técnica promissora para a compreensão de eventos biológicos a partir da análise de diversos transcriptomas depositados em bancos de dados públicos. Essa abordagem permite não só avaliar quais genes são diferentemente expressos nas diversas condições, mas também é capaz de inferir sobre suas as respectivas vias biológicas ativadas após um determinado estímulo. Portanto, a AIT pode ser útil no estudo da interação nanopartícula-célula, pois pode ser que ela consiga identificar grupos de genes que possam relacionar o tipo de material, morfologia e carga utilizado nas NPs com a resposta celular.

É importante que estudos complementares possam ser feitos para entender e desenvolver conhecimentos sobre a interação nanopartícula-célula (KUNZMANN *et al*., 2011). Porém poucos estudos realizaram a comparação de dados obtidos por transcriptoma entre NPs e células diferentes, sendo essas informações essenciais para definir se o uso da nanopartícula na saúde humana é seguro e se os tratamentos aplicados a partir dessa tecnologia são eficazes (HUSSIEN *et al.*, 2013; PISANI *et al.*, 2015; WANG, LIYING *et al.*, 2014; WU *et al.*, 2019; ZENG *et al.*, 2016). Portanto, o estudo de transcriptomas de forma integrativa vai facilitar a identificação de biomarcadores específicos da interação nanopartícula-célula. Essa análise poderá identificar um grupo de genes que possam relacionar o tipo de material utilizado na nanopartícula com a resposta celular e assim, identificar genes e vias biológicas regulados por esta interação. Estas informações poderão ser

utilizadas no monitoramento das terapias baseadas em NPs ou na melhora da ação destas terapias.

ARTIGO - INTEGRATIVE TRANSCRIPTOME OF HUMAN CELLS TREATED WITH DIFFERENT TYPES OF NANOPARTICLES

João Francisco Vitório Rodrigues[1], Luiz Cosme Cotta Malaquias[1,] Luiz Felipe Leomil Coelho[1#]

1. Laboratório de Vacinas, Departamento de Microbiologia e Imunologia, Instituto de Ciências Biomédicas, Universidade Federal de Alfenas, Rua Gabriel Monteiro da Silva, 700, Alfenas, 37130-001, Brasil

#* Corresponding author:

Luiz Felipe Leomil Coelho
Laboratório de Vacinas
Instituto de Ciências Biomédicas
Universidade Federal de Alfenas
Rua Gabriel Monteiro, 700 Centro
Alfenas – Minas Gerais- Brazil
CEP: 37130-000
Phone: 55 35 37019569
E-mail: luiz.coelho@unifal-mg.edu.br

ABSTRACT

Nanoparticles (NPs) are defined as a particle of matter that is between 1 and 100 nanometers in at least one side. This technology has a promising potential for several biological applications due to its possibility of functionalization which allows the selective delivery of nanoparticles to organs, tissues, and cells. The applicability in human health is related to the use of NPs as stimulators of the immune system when they are conjugated with antigens, in the diagnosis and treatment of tumors, and also as delivery drugs systems to target organs and tissues. Despite the use of NPs in new diagnostic, treatment, and prevention technologies for human diseases, few studies are conducted to verify the effect of NPs on the cellular transcriptome. Integrative transcriptome analysis (ITA) is currently recognized as a promising technique for understanding biological events through the analysis of several transcriptomes deposited in public databases. In this research, 81 transcriptomes derived from human cells treated with nanoparticles were identified in the Gene Expression Omnibus (GEO) database. Of these, 45 were selected because they are transcriptomes of cells treated with nanoparticles composed only of one material (without association or conjugation with any other substance or material) and untreated cells. Due to the variability of these studies, only transcriptomes of cells treated with NPs for 24 hours were selected. Thus, 30 datasets were used and these comprising transcriptomes derived from 5 materials and 6 different cells. ITA used the differentially expressed genes (DEGs) in each of the transcriptomes and demonstrated specificity in the cellular response to different types of NPs. Few DEGs were common on two or more analyzed transcriptomes. The analysis of biological pathways showed a high diversity of biological pathways that were activated or suppressed by the different treatments and also a very low number of shared pathways among the transcriptomes. Therefore, the ITA of human cell transcriptomes treated with different nanoparticles demonstrates a specific transcriptional response to material and also to the cell type.

.

1 INTRODUCTION

Nanotechnology and its application in medicine have given rise to a new field called nanomedicine (PAUTLER; BRENNER, 2010). This field has emerged as a consequence of the challenges encountered for the development of new vaccines, new diagnostics, and also new finds to deliver more efficient drugs and antigens (PAUTLER; BRENNER, 2010). This new nanotechnology approach has been revolutionized medicine (BAWARSKI *et al.*, 2008) and despite the advances attributed to the use of NPs, few studies aim to elucidate their bioaccumulation and risks derived from its use on human (WU *et al.*, 2019).

NPs are defined as a particle of matter that is between 1 and 100 nanometers (nm) in at least one side. They can be made of different materials and could have chemical, structural, mechanical, electrical, or biological characteristics different from their bulk material. NPs can be produced from metals, lipids, polymers, silica, proteins, and carbon (WOLFRAM *et al.*, 2016). They can present diverse morphologies and the most common are nanoshells, nanorods, liposomes, dendrimers, spheres, discs, cylinders, cones, tubes, and wires (VENTOLA; BHARALI; MOUSA, 2010). There are several benefits of using NPs in medicine. As example, the use of quantum dots and magnetic NPs can increase the sensitivity of image diagnostics. NPs can be also used to deliver genes and drugs to target cells (MURTHY, 2007). Therefore the use of this technology to treat cancer, chronic and infectious diseases is gaining attention in the last years (PATRA *et al.*, 2018).

Study the cellular response for each type of nanoparticle is necessary to determine the safety and also to define risks when using this technology, both in short-term treatments and also on prolonged exposure (KUNZMANN *et al.*, 2011; MAYNARD, 2012). *In vivo* tests are a valuable tool to assess the toxicity of a molecule, however, the toxicity of NPs mediated by their physical and chemical properties, such as size, shape, surface charge raises ethical and financial questions since each variable must be considered and the demand for animals would be considerably high (KOOTER *et al.*, 2019). Thus, *in vitro* studies have become a more viable alternative since it could be used to test several formulations of NPs in several different cells. This is in agreement with the concept of 3R (RUSSELL; BURCH, 1959).

The “omics” technologies (genomics, transcriptomics, proteomics, and metabolomics) are a set of robust methodologies used to assess the cellular response to a specific stimulus at the molecular level (KARCZEWSKI; SNYDER, 2018). Transcriptome presents a view of what are transcripted in the cell, being transcriptome the sum of all the transcripted gene. Measuring gene expression gives information on how genes are regulated and reveal details of the organism's biology. This information can help to infer functions from certain genes and could be an instrument to understand human pathologies (LOWE *et al.*, 2017). Currently, two techniques are more used to study the transcriptome,

the microarray, and RNA sequencing (RNAseq). The RNAseq is better than microarray because can map the entire transcriptomes on any organism (WANG, ZHONG; GERSTEIN; SNYDER, 2009). Therefore, its use has increased over the microarray in recent years (LOWE *et al.*, 2017).

Complementary studies must be done to understand the interaction of NPs and cells and this could be important to develop knowledge about the nanoparticle-cell interaction and also on nanotoxicology (KUNZMANN *et al.*, 2011). The identification of DEGs on cells treated with NPs could be important to measure the cell response to nanoparticle treatment. Therefore, this work aimed to use bioinformatics tools to analyze, in an integrated way, a series of transcriptome data and therefore identify genes and/or biological pathways induced in human cells after nanoparticle treatment.

2 METHODS

2.1 TRANSCRIPTOME DATA OF NANOPARTICLE TREATED CELLS

Gene expression profiling data from nanoparticle treated human cells were retrieved from Microarray data from the Gene Expression Omnibus (GEO) platform (https://www.ncbi.nlm.nih.gov/gds) using the term “nanoparticles”. Information about the number of samples used in each experimental condition, time of treatment, cell type, tissue origin, nanoparticle material, nanoparticle morphology, the methodology used for transcriptomic analysis, platform, and GEO identification number were collected and tabulated in an xls spreadsheet (Supplementary Table 1). Only studies performed with at least two replicates for each experimental sample were included. In order to verify the effect of the nanoparticle material on cells, only data from untreated cells and NPs treated cells were used for comparison. Data derived from experimental conditions that used NPs associated with other compounds (ex: drugs or proteins) to treated cells were excluded from the next analysis. In this study, each dataset was processed using the GEO2R online software (https://www.ncbi.nlm.nih.gov/geo/) to compare untreated and nanoparticle treated cells samples to screen DEGs. The *t test* and Benjamini and Hochberg method were used to calculate the *P* values and false discovery rate, respectively. Genes that were differentially expressed between the two conditions were screened with the threshold value of $p < 0.05$. The final list of 250 differential expressed genes was annotated on an xls spreadsheet.

2.2 NETWORK CONSTRUCTION

All networks presented in this work were built using Gephi version 0.9.2 (Bastian and Heymann, 2009). The cells and genes were listed in a comma-separated values (.csv) spreadsheet for each graph, and this file was imported into the software. Another .csv spreadsheet with the connections was also imported to generate the network graph. In all networks, the node diameter is

directly proportional to the edge degree. The layout was generated using algorithms based on the force of attraction and repulsion of the nodes (Fruchterman Reingold). Class modularity was applied to define clusters and if necessary, the nodes were submitted to local rearrangement for better visualization of the connections between nodes.

2.3 PATHWAY ANALYSES

The Enrichr platform (http://amp.pharm.mssm.edu/Enrichr/) was used to study pathway enrichment analyses of DEGs (Kuleshov *et al*., 2016). The database used for pathway enrichment analysis was Kyoto Encyclopedia of Genes and Genomes (KEGG). An adjusted $p \leq 0.05$ was considered statistically significant for all analyses. The lists of significant pathway terms were recorded on a xls spreadsheet.

3 RESULTS

3.1 GENERAL CHARACTERISTICS OF TRANSCRIPTOME STUDIES DERIVED FROM NANOPARTICLES TREATED HUMAN CELLS

Based on a bioinformatics approach this study aims to identify differed DEGs induced on human cells after nanoparticle treatment. A search of relevant studies that have transcriptome data from human nanoparticle treated cells was done in the GEO database until December 12, 2019. The initial search using the term “nanoparticles” retrieved 244 studies. The *Homo sapiens* filter was applied and as result, the number of studies was reduced to 81 studies. Each study was analyzed individually to identify if they met the inclusion criteria previously described in the Methods section and a final list of 45 studies were obtained (Figure 1). Among these studies, it was identified 5 studies that used RNA-sequencing and 40 studies that used Microarray (Figure 2a). Time analysis indicates a high number of microarrays in the past with a tendency to use RNAseq after 2017 (Figure 2b).

Analysis of experimental parameters indicates that the transcriptome studies used 19 different types of materials to produce NPs, being carbon the most used material followed by titanium and zinc (figure 3a). The 37 different types of human cells used on all described experimental procedures were grouped into 7 biological systems according to their origin. Cells derived from the immune system was the most frequent experimental protocol used on these transcriptome studies (44%) (Figure 3b). The reproductive, respiratory, and digestive systems represented 19% 18%, 12% of studies, respectively. The other systems (integumentary, nervous, and ocular) represented only 8% (figure 3b).

A bipartite network graph was constructed to better represent the type of material used to develop NPs and the target biological system. The size of the nodes in biological systems and the thickness of the edges represent the degree of interaction. Therefore, a greater node or edge representation

indicates a higher number of experimental protocols performed. Among the biological systems identified, the immune system had the highest number of transcriptome studies with 37 different experimental protocols. Thirteen different types of NPs were identified, being carbon, zinc, and titanium NPs the most used. Cells derived from the respiratory system were used to generate transcriptome studies using 8 different NPs, being the carbon, silica, and zinc the most used. Regarding cells derived from the reproductive system, it was identified 9 different types of NPs. In this case, carbon and silver NPs were the most used. Cells derived from the digestive system were treated with 8 different nanoparticle types. Titanium, zinc, and galactoxyloglucan polysaccharide (PST-DOX) were the most used NPs in this case. Cells from the integumentary system were treated with 3 different types of NPs and cells from ocular and nervous systems were treated with gold and polyamidoamine dendrimer (PAMAM) NPs, respectively (figure 3c). In general, the studies used a prolonged time of treatment, being the 24 and 48 hours the most frequent (Supplementary Table 1).

3.2 DIFFERENTIAL EXPRESSED GENES ON NANOPARTICLE TREATED CELLS

To identify genes that were differentially expressed between untreated and nanoparticle treated cells the Geo2r tool was used. The 45 selected studies have several differential experimental conditions, such as cell type, time of treatment, type of material, nanoparticle concentration, and nanoparticle morphology. Due to the high variability of these parameters, only datasets from cells treated with nanoparticle for 24 hours were used on the next steps of integrative analysis. After using this parameter of selection, only datasets from cells treated with carbon, gold, silver, titanium, and zinc for 24 hours were submitted to the identification of DEGs. The 250 DEGs (upregulated and Downregulated) from each dataset were exported to an xls spreadsheet and the results were represented in table 1. Downregulated and upregulated genes list from datasets were uploaded to Bioinformatics & Evolutionary Genomics Genomics Tools (bioinformatics.psb.ugent.be/webtools/venn) and the shared DEGs between the datasets were identified (supplementary table 2).

The final lists containing the identified DEGs from each type of material were used to build bipartite network graphs to better represent the effect of nanoparticle treatment on each cell type. The bipartite networks showed in figure 4 and 5 indicate that were few shared DEGs between cells treated with the same type of nanoparticle material. In general, it was observed a specific transcriptional response for each dataset with few DEG shared by two or more studies (Figure 4 and 5, Table 2, and supplementary table 2). As the integrative analysis using different cells and the same nanoparticle material showed few shared DEGs, it was performed a new set of analyses to verify the effect of different NPs on the same cell line (Figure 6 and 7). Caco2 and MCF7 cells had the highest of number of transcriptomes studies and therefore the highest number of shared DEG (Table 3). HMDM, MDDC, HHC-LM3, HET1A, HEPG2

and HUVEC cells were excluded from this analysis due to lack of gene sharing between two or more datasets. Therefore, it was possible to verify a high number of DEGs between the different nanoparticle treatments on these cells.

3.3 BIOLOGICAL PATHWAY ENRICHMENT ANALYSES OF DEGS

Pathway enrichment analysis using the upregulated and downregulated DEGs indicates that are a high number of biological pathways regulated by nanoparticle treatment on these cells (Table 1). Supplementary table 3 contains a complete list of all biological pathways activated or suppressed in each treatment. Thus, a total of unique 85 downregulated and 57 upregulated pathways were regulated by NPs treatment when the ITA was performed using the material as the main criteria of analysis (Figure 8). The numbers of unique and shared biological pathways identified by integrative analysis of different cell types treated with NPs made by the same material were described on table 4. Table 5 showed the number of biological pathways identified by integrative analysis of the same cell type treated with NPs made by different materials. In this case, it was detected 79 downregulated and 57 upregulated pathways (Figure 8). It is important to note that the difference in the total of identified pathways between the ITA using material and cells as main criteria is due to to the exclusion of HMDM, MDDC, HHC-LM3, HET1A, HEPG2 and HUVEC cells derived datasets. These cells had only one dataset and therefore it is impossible to perform a ITA analysis. Data presented on both tables show a low number of shared biological pathways regulated by nanoparticle treatment.

Among the downregulated pathways shared by different cells types treated with NPs made by different materials that were, cells treated with carbon NPs presented only 1 pathway shared between 2 datasets. Cells treated with silver NPs presented 7 pathways shared between 2 datasets, 32 pathways shared between 3 to 5 datasets and 6 pathways shared between 6 or more datasets. Cells treated with titanium and zinc NPs presented 1 pathway shared between 2 datasets respectively. Among the upregulated pathways it was detected only 1 shared pathway between 2 datasets on cells treated with carbon NPs and 4 on cells treated with Silver NPs. Only 2 upregulated pathways were shared by 3 or 5 datasets on cells treated with silver NPs.

When the analysis was done using the same cell type treated with NPs made by different materials the results are very similar. Among the downregulated pathways shared by cells, CACO2 cells presented 5 pathways shared between 2 datasets and 37 pathways shared between 3 to 5 datasets. JURKAT cells presented 1 pathway shared between 2 datasets. MCF7 cells presented 2 pathways shared between 2 datasets and 4 pathways shared between 3 to 5 datasets. THP1 cells presented 18 pathways shared between 2 datasets. Among the upregulated pathways CACO2 cells presented 8 pathways shared between 2 datasets and 2 pathways shared between 3 to 5 datasets. MCF7 cells presented 4 pathways shared between 2 datasets. 16LU and SAE cells did not present pathways shared between datasets.

4 DISCUSSION

Nanomedicine is a new and emerging subject of research that aims to use nanotechnology with the pharmaceutical and biomedical sciences. The main purpose of nanomedicine is to use NPs to find new ways to deliver drugs and antigens, performing diagnosis, and improve safety and toxicity (Ventola, 2012). Besides the importance of nanotechnology, it is unclear the effect of NPs on cells, especially on gene expression. Study the cellular response for each type of nanoparticle is necessary to determine the safety and to define risks using this technology. After an extensive search on the GEO database, it was identified transcriptome datasets from nanoparticle treated human cells (Figure 1 and 2). Besides the high number of datasets identified (n=244) only a few fully met the inclusion criteria (n=45). This data shows that there was negligence in studying the transcriptional response in cells treated with NPs.

The genome comprises the information for all biological functions on living cells. However, the genome alone is not able to deliver this information to the cell, and therefore, it is necessary a coordinated action of enzymes and proteins to generate gene expression. The first product of these reactions is defined as transcriptomes and it is defined as a set of all the transcribed mRNA molecules on cells. Currently, two techniques are used to study the transcriptome and these are the Microarray and RNA sequencing (RNAseq) (LOWE *et al.*, 2017; RANI; SHARMA, 2017). Microarrays measure the abundances of a predetermined set of transcripts via their hybridization to an array of complementary probes in a solid substrate (HELLER, 2002). Each probe corresponds to a known mRNA and the hybridization of a cDNA to these probes is detected by a fluorescent signal. RNAseq is a technology that converts RNA in a library of cDNA with an adaptor in one or both ends for large-scale sequencing (WANG, ZHONG; GERSTEIN; SNYDER, 2009). The RNAseq has grown in popularity since it can generate more information about the transcriptome than microarray (LOWE *et al.*, 2017). Another advantage of RNAseq if compared to microarray is the non-limitation of this technique to model organisms since it can be used in organisms with unknown genomic sequences (WANG, ZHONG; GERSTEIN; SNYDER, 2009). As observed, most studies have been carried out with microarray, but there has been a trend towards the use of RNA-seq in recent years as shown in figure 2b. However, there are few studies carried out with both technologies, which may hinder the use of NPs for the development of new treatments.

The formulation of the nanoparticle is an important point to be considered, since the type of material used and also its shape and size can influence bio-distribution and trigger several biological processes like modulation of gene expression, systemic and local immune response, tissue proliferation, ion transport cytotoxicity, cellular stress and apoptosis (SOTO; GARZA; MURR, 2007; WU *et al.*, 2019). Regarding the biological origin of cells used on transcriptomes studies, it was observed a high frequency of studies that used cells derived from immune, respiratory and digestive systems (Figure 3b). Several types of NPs were used to treat cells with a high frequency of carbon,

iron, titanium, zinc, and silver NPs. Carbon NPs are widely used as drug and gene delivery systems targeting tissues and cells (KUSHWAHA *et al.*, 2013, KHAN; SAEED; KHAN, 2017). Iron oxide NPs have been used as an adjuvant option for the treatment of several cancers helping chemotherapy and radiotherapy (COURT *et al.*, 2017). Molecular imaging using antibody-conjugated gold NPs and superparamagnetic iron oxide NPs are also described (MA *et al.*, 2016, ADAY *et al.*, 2014). Silver and titanium NPs have antimicrobial properties and can be used as disinfectants (BÖHMERT *et al.*, 2015, JANG, 2016, KAWATA; OSAWA; OKABE, 2009, VERMA; GANGWAR; SRIVASTAVA, 2017). Zinc NPs can protect against broad-spectrum UV radiation and are present in cosmetic products with sunscreen characteristics (OSMOND MCLEOD, 2014).

The integrative analysis of transcriptomes derived from carbon, gold, silver, titanium, and zinc nanoparticle treated cells showed a specific cell response after nanoparticle treatment (table 2, figure 4 and 5). Similar results were found when immune-competent human cells (Human monocyte-derived dendritic cell, Human monocyte-derived macrophages, and Jurkat) were treated with zinc oxide and titanium oxide NPs (TUOMELA *et al.* 2013). The same observation was done by VAN DER ZANDE *et al.* (2016). In this case, the authors studied the transcriptomes of two different cells (CACO2 and MCF-7) treated with silver NPs. Besides the detection of a differential transcriptional response, it was detected a common functional response related to oxidative stress. In the same way, Human Dermal Fibroblasts and human prostate cancer cell lines (PC3 cells) when exposed to gold NPs showed a different set of DEGs (GRZINCIC *et al.*, 2015). SAE, Caco-2, and THP1 cells treated with carbon and titanium dioxide NPs also showed a specific response to treatment. Cells treated with carbon NPs showed up-regulation of genes involved in cell proliferation, anti-apoptotic pathway, and DNA repair while cells treated with titan NPs showed an inflammatory response associated with cellular stress (TILTON *et al.*, 2014).

When the integrative transcriptome analysis was done using a unique cell line treated with different NPs, it was also observed a nanoparticle specific cellular response with few shared DEGs (table 3, figure 6 and 7). This response could be associated with the chemical and physical characteristics of each nanoparticle. Even if the same material was used, the transcriptional response could be dependent on other nanoparticle parameters such as size, morphology, and surface charge that (GRZINCIC *et al.*, 2015; JANG, 2016; THAI *et al.*, 2016)

The pathway enrichment analysis of DEGs demonstrated a high number of downregulated pathways when compared to the upregulated pathways (figure 8). This data indicates that in general, the treatment of cells with NPs has a huge potential to inhibit some biological pathways. However, it is not possible to make a clear correlation between the type of nanoparticle and the biological response to this treatment since both upregulated and downregulated biological

pathways are related to cancer, infection, cell signaling, immune system and metabolism (Supplementary table 3). Once these NPs could be used to treat some diseases, it is important to evaluated which biological pathways are activated on the target cell after nanoparticle treatment and if this treatment could be deleterious to another cell/tissue/organ. Therefore, our data indicate that the cellular response could be unique to each cell-nanoparticle interaction and efforts should be done in order to characterize the cellular response to nanoparticle treatment, especially when the nanoparticle was used to deliver drugs, proteins or antigens to a specific cell. Therefore, this analysis showed that a large number of biological pathways were identified and this number is influenced by the type of nanoparticle and also by the cell type.

5 CONCLUSION

In conclusion, integrative transcriptome analysis of human cells treated with NPs showed that particular response to nanoparticle treatment is evident in each cell type since most genes and biological pathways identified in a specific cell type were not present in another type. So, it is recommended that when new NPs were developed for use on human, different cells should be tested to ensure the efficacy and safety of these NPs in humans.

Figure 1- Flowchart detailing the selection of studies included in the integrative transcriptome analysis**.**

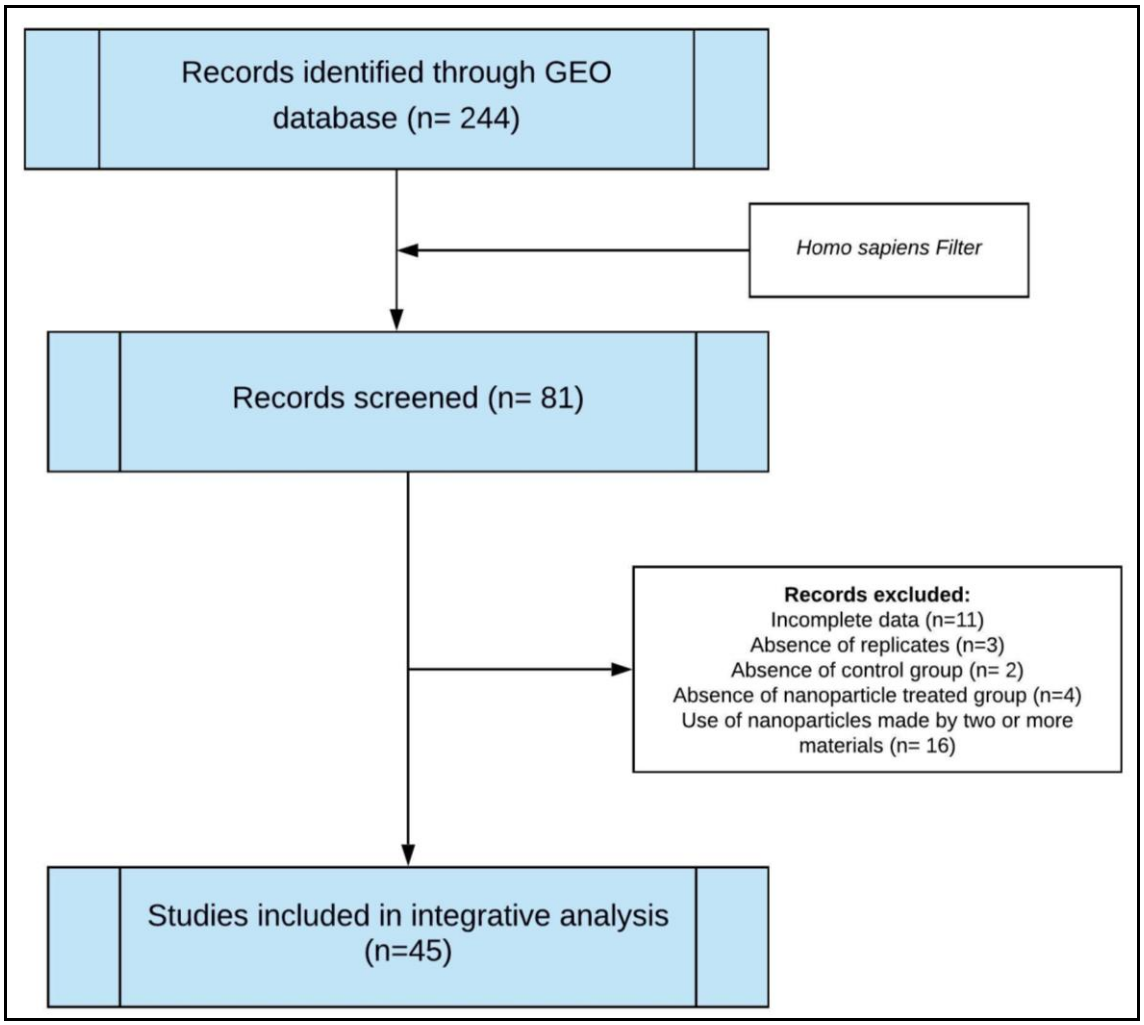

Author's source (2020).

Figure 2- Transcriptome studies derived from nanoparticle treated human cells. (A) Type of technology used to generate transcriptome data. (B) A time lime graph showing the number of microarray and RNAseq transcriptome studies derived from human cells treated with NPs.

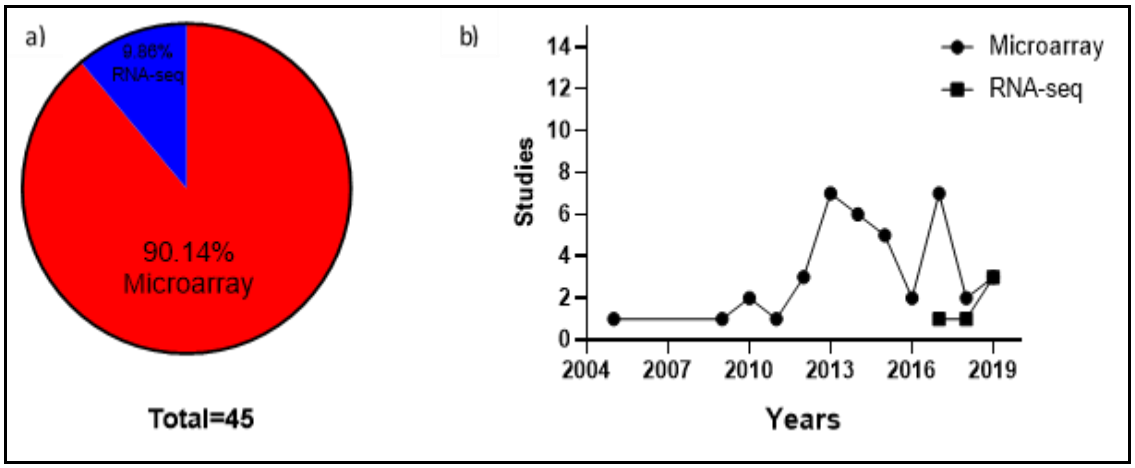

Author's source (2020).

Figure 3. General characteristics of all transcriptome studies used in the integrative analysis. A) Types of material used to produce NPs. B) Target biological systems used to produce transcriptome from NPs human treated cells. C) Bipartite network graph showing a spatially connected network among the type of material used to develop NPs and the target biological system. Each node represents a biological system or the type of nanoparticle material. The layout was generated using a force-based algorithm followed by manual rearrangement for better visualization of the connections. Acronyms: HANPs – Hydroxyapatite, PLGA - Poly-lactic-co-glycolic acid, PAMAM - polyamidoamine dendrimer, PBAE447 - β-amino esters 447, PMMAEA - ethyl acrylate-co-methyl methacrylate-co-trimethylammonioethyl methacrylate chloride, PST-DOX-Galactoxyloglucan polysaccharide.

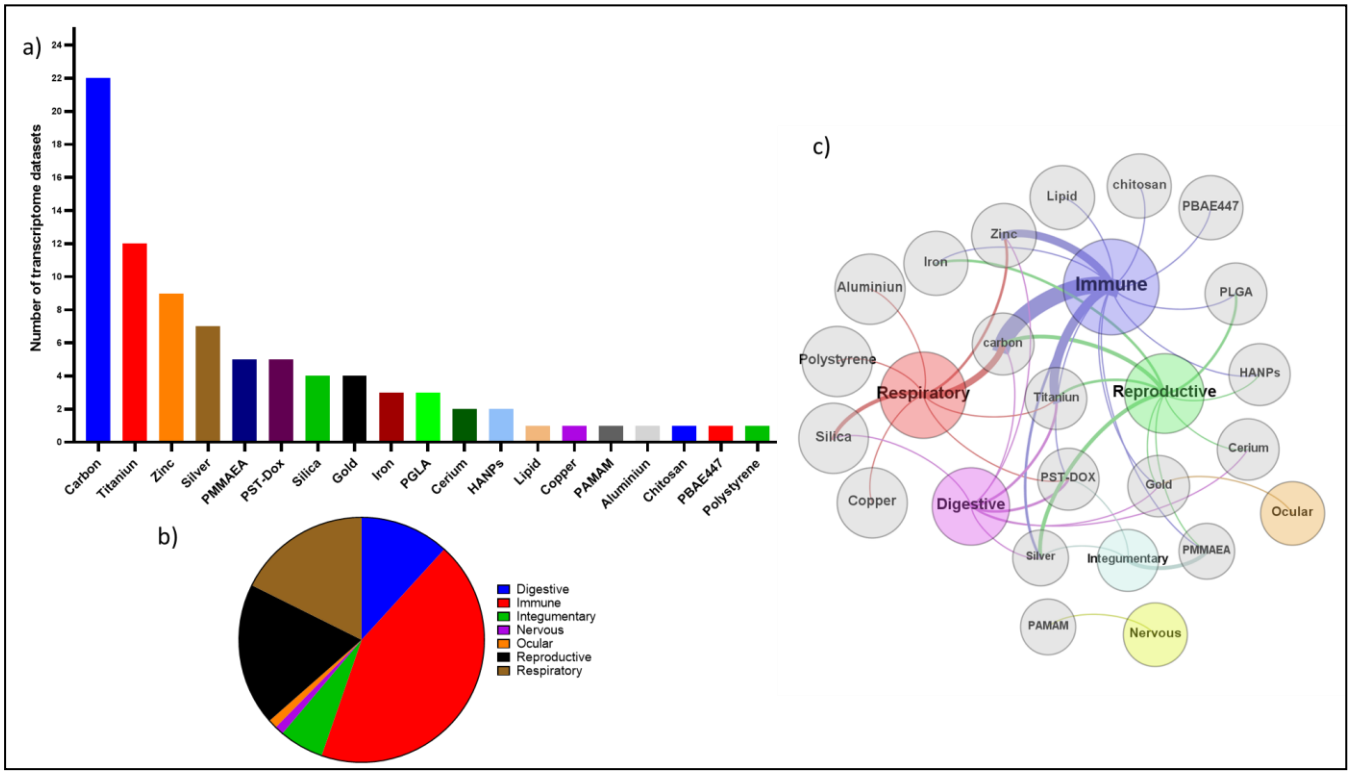

Author's source (2020).

Figure 4. The network of up and downregulated genes after nanoparticle treatment of different cell types. Carbon, Gold and Silver bipartite network graph shows a spatially connected network among DEGs and cell types after nanoparticle treatment. Each node represents a nanoparticle or cell type and each cluster of DEG cell responses represented by a different color.

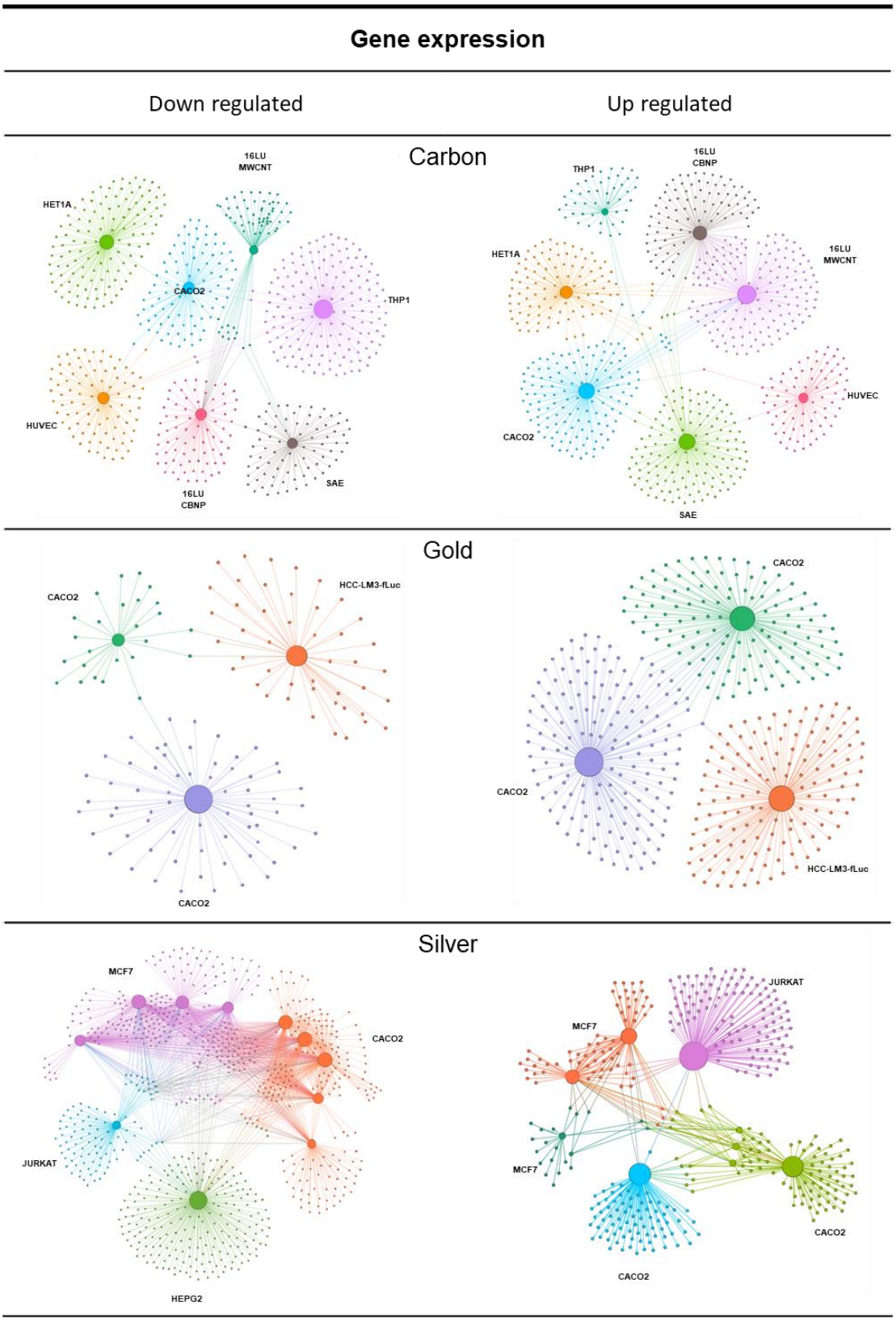

Author's source (2020).

Figure 5. The network of up and downregulated genes after nanoparticle treatment of different cell types. Titanium and Zinc bipartite network graph shows a spatially connected network among DEGs and cell types after nanoparticle treatment. Each node represents a nanoparticle or cell type and each cluster of DEG cell responses represented by a different color.

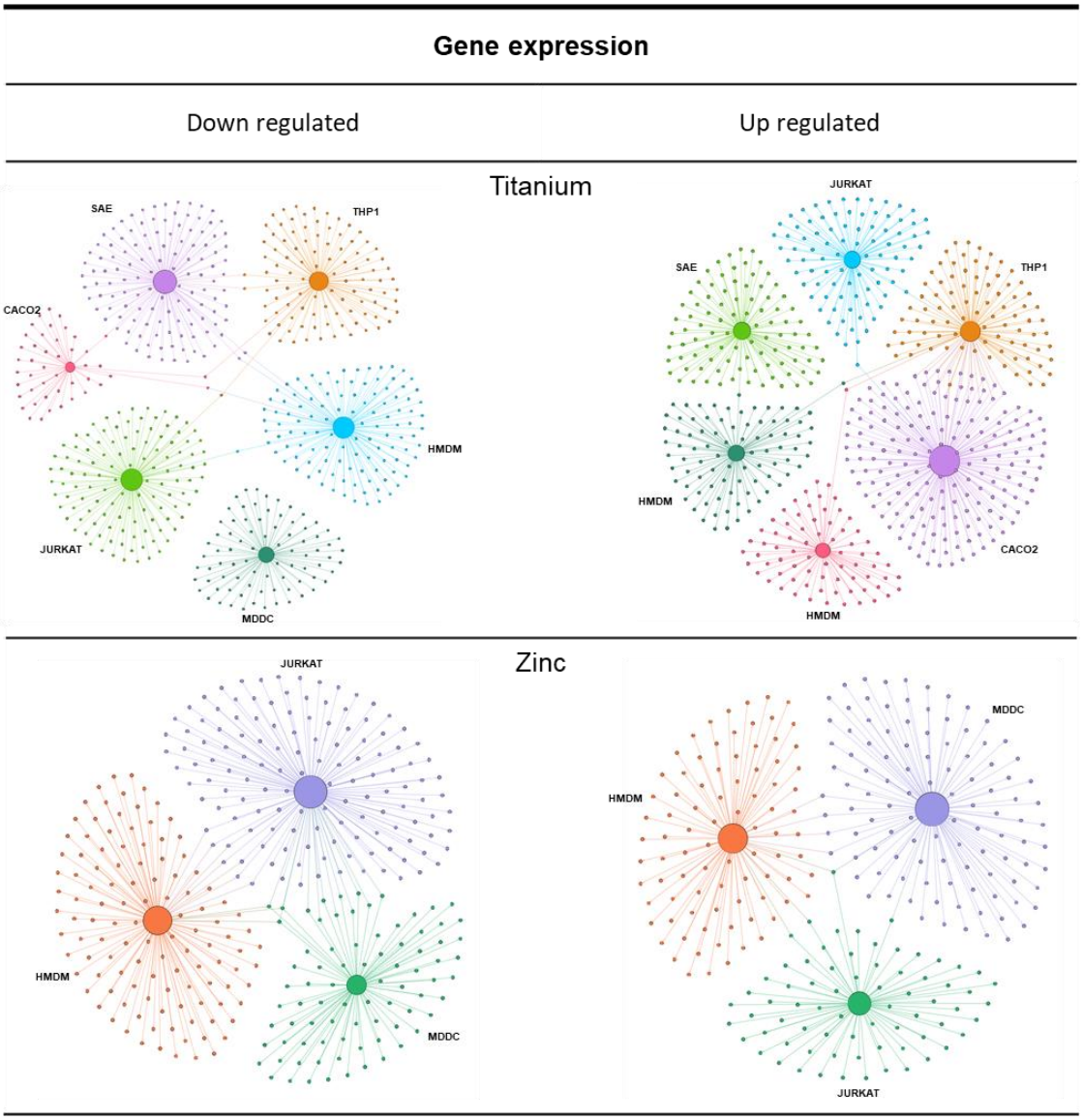

Author's source (2020).

Figure 6. The network of up and downregulated genes of cells treated with different types of NPs. 16LU, CACO2 and JURKAT bipartite network graph shows a spatially connected network among DEGs and cell types after nanoparticle treatment. Each node represents a nanoparticle or cell type and each cluster of DEG cell responses represented by a different color.

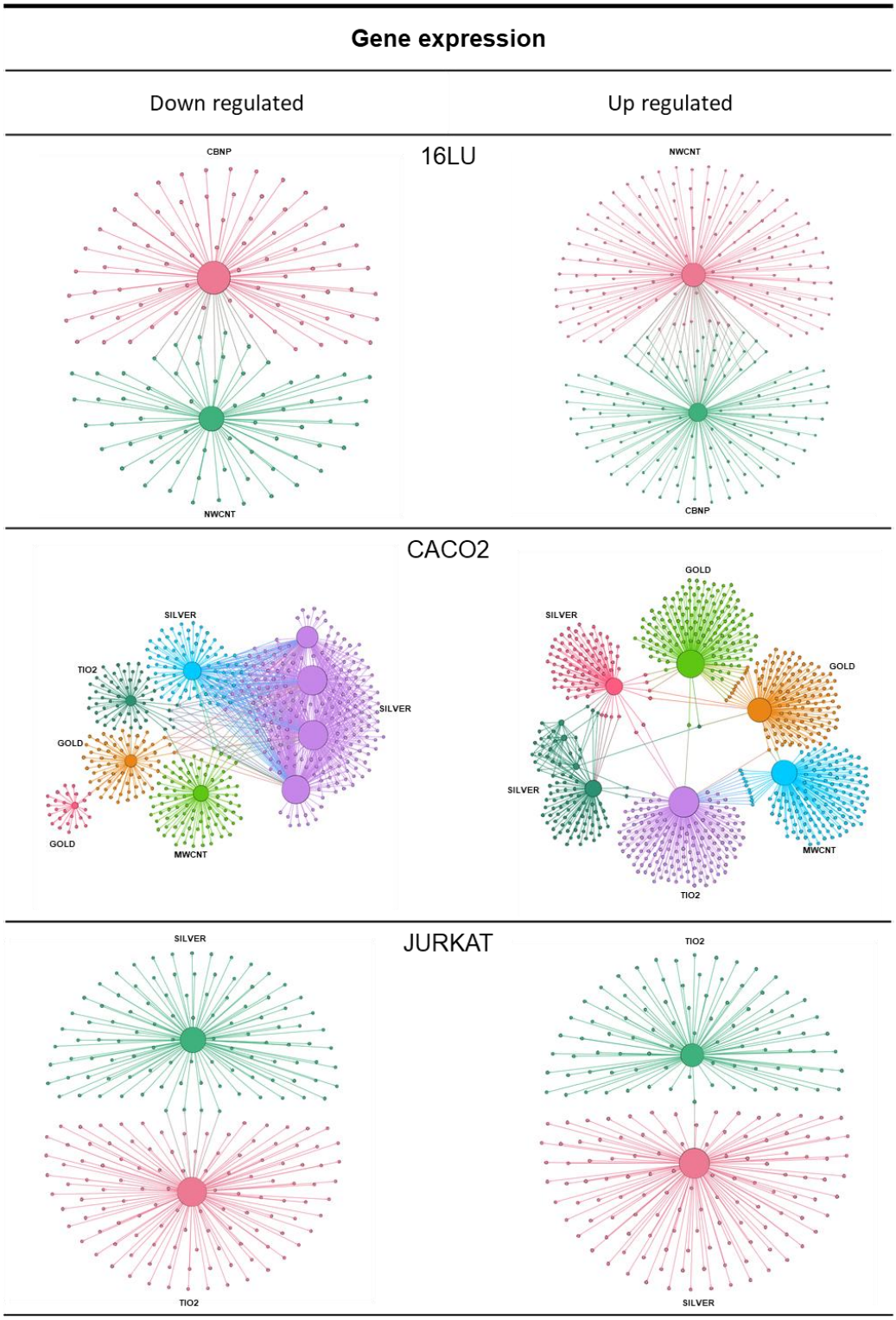

Author's source (2020).

Figure 7. The network of up and downregulated genes of cells treated with different types of NPs. MCF7, SAE and THP1 bipartite network graph shows a spatially connected network among DEGs and cell types after nanoparticle treatment. Each node represents a nanoparticle or cell type and each cluster of DEG cell responses represented by a different color.

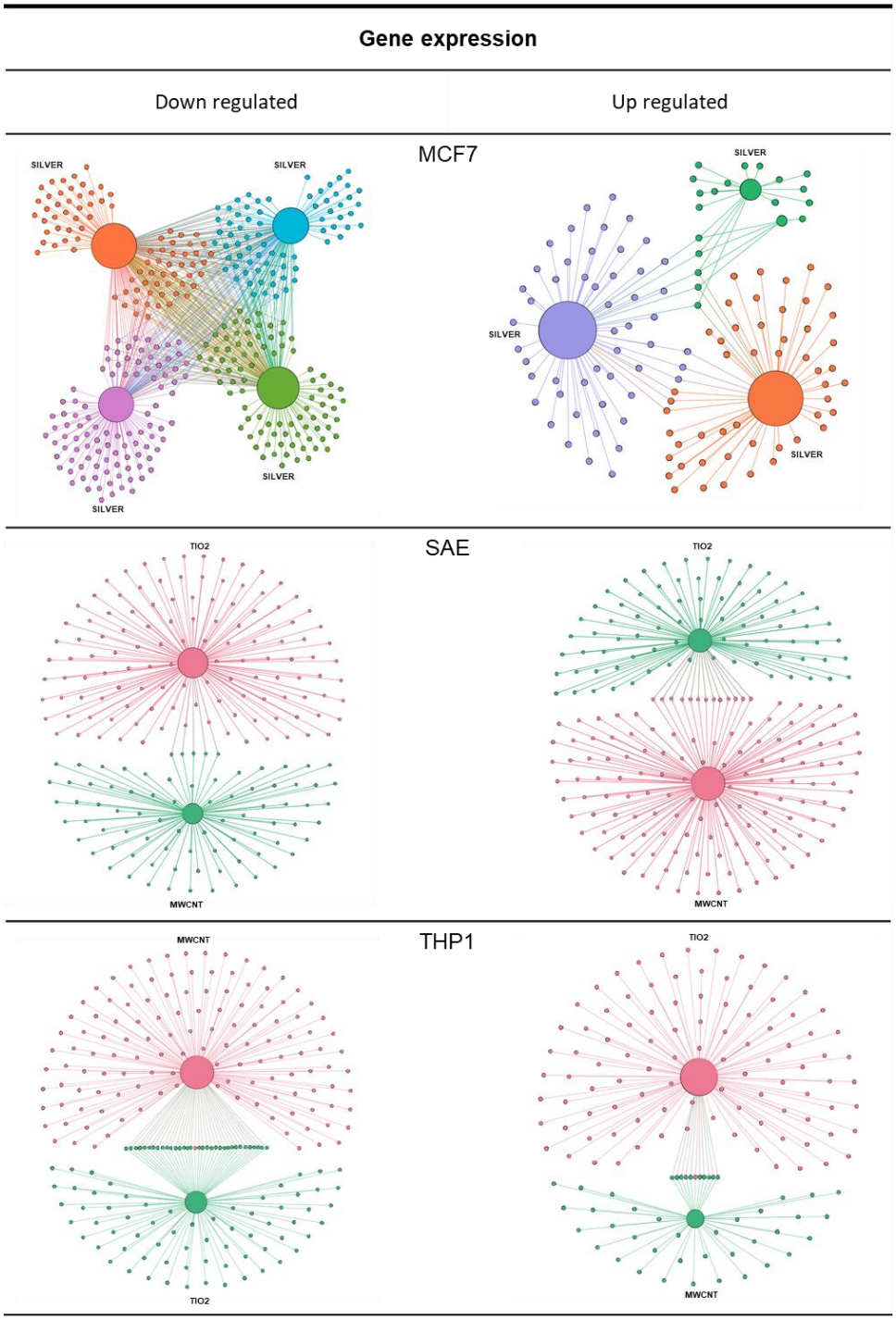

Author's source (2020).

Figure 8. Pathway enrichment analysis of DEG`s showing the number of unique biological pathways using Enrichr platform. Kyoto Encyclopedia of Genes and Genomes was used to identifiy each pathways and those with ajusted p value <0.05 were considered.

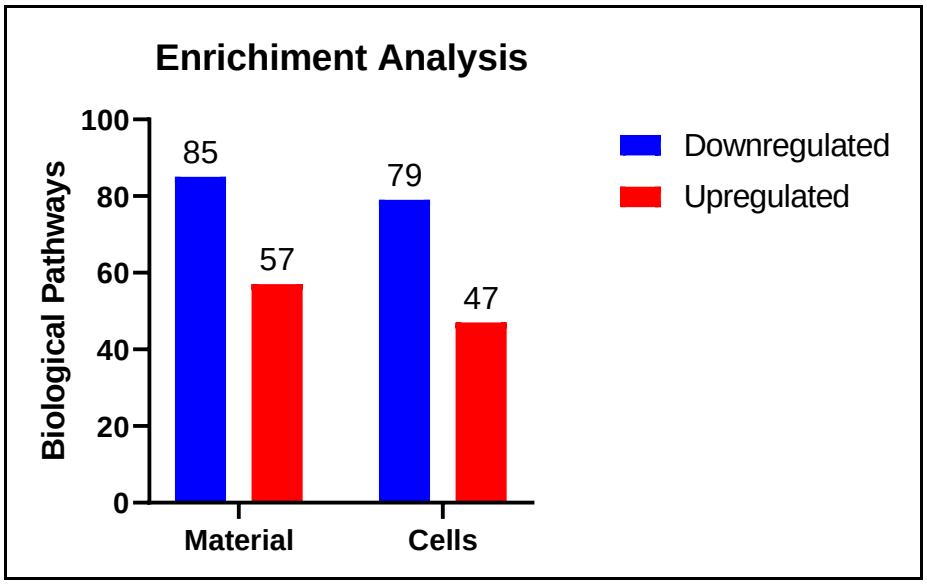

Author's source (2020).

Table 1: Number of DEGs and biological pathways among NPs treated cells.

Material	Dataset	Cell Type	NP Morphology	NP Size	Downregulated DEG	Downregulated Pathways (P-value< 0.05)	Upregulated DEG	Upregulated Pathways (P-value<0.05)
Carbon	GSE3364	HUVEC	Spherical	4,7-9,5nm	99	1	77	0
	GSE43515	16LU	Spherical	Not reported	100	2	142	2
	GSE43515	16LU	Nanotube	Not reported	69	3	178	11
	GSE42066	CACO2	Nanotube	5-10x20-30nm	93	0	147	0
	GSE42067	SAE	Nanotube	5-10x20-30nm	81	0	141	0
	GSE42068	THP1	Nanotube	5-10x20-30nm	191	28	59	0
	GSE96720	HET1A	Spherical	4-6nm	123	0	106	0
Gold	GSE55349	CACO2	Spherical	5nm	66	0	158	0
	GSE55349	CACO2	Spherical	40nm	25	0	133	0
	GSE59284	HCC-LM3	Spherical	5nm	49	0	145	0
Silver	GSE84982	CACO2	Spherical	110nm	141	24	89	0
	GSE84982	MCF7	Spherical	110nm	191	4	17	0
	GSE84982	CACO2	Spherical	60nm	211	43	19	0
	GSE84982	MCF7	Spherical	60nm	210	6	5	0
	GSE84982	CACO2	Spherical	30nm	206	45	22	2
	GSE84982	MCF7	Spherical	30nm	163	4	56	5
	GSE84982	CACO2	Spherical	20nm	200	35	25	2
	GSE84982	MCF7	Spherical	20nm	158	11	68	5
	GSE62253	CACO2	Spherical	15-28nm	135	11	100	0
	GSE14452	HEPG2	Not reported	7-10nm	246	11	0	0
	GSE20692	JURKAT	Spherical	<100nm	106	5	125	25
Titanium	GSE39316	HMDM	Spherical	27,4-35,2nm	122	0	73	0
	GSE39316	JURKAT	Spherical	27,4-35,2nm	119	0	88	0
	GSE39316	MDDC	Spherical	27,4-35,2nm	82	0	86	0
	GSE42066	CACO2	Nanobelts	7x0,2x001nm	39	0	202	6
	GSE42067	SAE	Nanobelts	7x0,2x001nm	140	2	96	1
	GSE42068	THP1	Nanobelts	7x0,2x001nm	128	29	121	1
Zinc	GSE39316	HMDM	Spherical	13-16,4nm	132	1	97	11
	GSE39316	JURKAT	Spherical	13-16,4nm	156	1	73	0
	GSE39316	MDDC	Spherical	13-16,4nm	81	1	109	0

Author's source (2020).

Table 2 - Number of DEGs identified by integrative analysis of different cell types treated with NPs made by the same material.

Material	Datasets	Cells types	Downregulated Total	Downregulated Shared[1]	Upregulated Total	Upregulated Shared[1]
Carbon	7	6	756	19	850	57
Gold	3	2	140	3	436	12
Silver	11	4	1967	95	526	25
Titanium	6	6	630	9	666	26
Zinc	3	3	369	20	279	9

1: DEGs shared by two or more datasets.
Author's source (2020).

Table 3: Number of DEGs identified by integrative analysis of cells treated with NPs made by different materials.

Cell type	Datasets	Nanoparticle Material	Downregulated Total	Downregulated Shared[1]	Upregulated Total	Upregulated Shared[1]
16LU	2	1	169	11	320	34
CACO2	9	4	1116	203	895	58
JURKAT	2	2	381	4	286	1
MCF7	4	1	722	165	146	11
SAE	2	2	221	4	237	13
THP1	2	2	319	34	180	11

1: DEGs shared by two or more datasets.
Author's source (2020).

Table 4. Number of biological pathways identified by integrative analysis of different cell types treated with NPs made by the same material.

Material	Datasets	Cells types	Pathways Downregulated Total	Pathways Downregulated Shared by 2 datasets	Pathways Downregulated Shared by 3 to 5 datasets	Pathways Downregulated Shared by 6 or more datasets	Pathways Upregulated Total	Pathways Upregulated Shared by 2 datasets	Pathways Upregulated Shared by 3 to 5 datasets	Pathways Upregulated Shared by 6 or more datasets
CARBON	7	6	33	1	0	0	13	1	0	0
GOLD	3	2	0	0	0	0	0	0	0	0
SILVER	11	4	64	7	32	6	31	4	2	0
TITANIUM	6	6	30	1	0	0	8	0	0	0
ZINC	3	3	2	1	0	0	11	0	0	0

Author's source (2020).

Table 5. Number of biological pathways identified by integrative analysis of the same cell type treated with NPs made by different materials.

Cell type	Datasets	Nanoparticle Material	Pathways Downregulated Total	Pathways Downregulated Shared by 2 datasets	Pathways Downregulated Shared by 3 to 5 datasets	Pathways Downregulated Shared by 6 or more datasets	Pathway Upregulated Total	Pathways Upregulated Shared by 2 datasets	Pathways Upregulated Shared by 3 to 5 datasets	Pathways Upregulated Shared by 6 or more datasets
16LU	2	1	5	0	0	0	13	0	0	0
CACO2	9	4	51	5	37	0	8	2	0	0
JURKAT	2	2	5	1	0	0	25	0	0	0
MCF7	4	1	11	2	4	0	6	4	0	0
SAE	2	2	2	0	0	0	1	0	0	0
THP1	2	2	39	18	0	0	1	0	0	0

Author's source (2020).

REFERENCES

ADAIR, Brian M. Nanoparticle vaccines against respiratory viruses. *Wiley Interdisciplinary Reviews: Nanomedicine and Nanobiotechnology*, v. 1, n. 4, p. 405–414, 2009.

ADAY, Sezin *et al.* Inflammatory modulation of stem cells by Magnetic Resonance Imaging (MRI)-detectable nanoparticles. *RSC Advances*, v. 4, n. 60, p. 31706–31709, 2014. Disponível em: <http://dx.doi.org/10.1039/C4RA04041D>.

BAWARSKI, Willie E. *et al.* Emerging nanopharmaceuticals. *Nanomedicine: Nanotechnology, Biology, and Medicine*, v. 4, n. 4, p. 273–282, 2008. Disponível em: <http://dx.doi.org/10.1016/j.nano.2008.06.002>.

BÖHMERT, Linda *et al.* Molecular mechanism of silver nanoparticles in human intestinal cells. *Nanotoxicology*, CACO2 - PRATA, v. 9, n. 7, p. 852–860, 2015.

BOUCHOUCHA, Meryem *et al.* Size-Controlled Functionalized Mesoporous Silica Nanoparticles for Tunable Drug Release and Enhanced Anti-Tumoral Activity. *Chemistry of Materials*, v. 28, n. 12, p. 4243–4258, 2016.

CHAKRABORTY, Sajib; RAHMAN, Taibur. The difficulties in cancer treatment. *Ecancermedicalscience*, v. 6, p. ed16, 2012.

COURT, Karem A. *et al.* HSP70 inhibition synergistically enhances the effects of magnetic fluid hyperthermia in ovarian cancer. *Molecular Cancer Therapeutics*, v. 16, n. 5, p. 966–976, 2017.

GRZINCIC, E. M. *et al.* Global transcriptomic analysis of model human cell lines exposed to surface-modified gold nanoparticles: the effect of surface chemistry. *Nanoscale*, v. 7, n. 4, p. 1349–1362, 2015. Disponível em: <http://xlink.rsc.org/?DOI=C4NR05166A>.

HELLER, Michael J. DNA microarray technology: Devices, systems, and applications. *Annual Review of Biomedical Engineering*, v. 4, p. 129–153, 2002.

HUSSIEN, Rajaa *et al.* Unique growth pattern of human mammary epithelial cells induced by polymeric nanoparticles. *Physiological Reports*, v. 1, n. 4, p. 1–17, 2013.

JANG, Jiyoung. *Increased interleukin-11 and stress genes in human endothelial and human bronchial epithelial cell lines by silver nanoparticles*. . Yonsei: [s.n.], 2016. Disponível em: <https://ir.ymlib.yonsei.ac.kr/handle/22282913/154921>.

KARCZEWSKI, Konrad J.; SNYDER, Michael P. Integrative omics for health and disease. *Nature Reviews Genetics*, v. 19, n. 5, p. 299–310, 2018. Disponível em: <http://dx.doi.org/10.1038/nrg.2018.4>.

KAWATA, Koji; OSAWA, Masato; OKABE, Satoshi. In vitro toxicity of silver nanoparticles at noncytotoxic doses to HepG2 human hepatoma cells. *Environmental Science and Technology*, v. 43, n. 15, p. 6046–6051, 2009.

KHAN, Ibrahim; SAEED, Khalid; KHAN, Idrees. Nanoparticles: Properties,

applications and toxicities. *Arabian Journal of Chemistry*, 2017. Disponível em: <http://dx.doi.org/10.1016/j.arabjc.2017.05.011>.

KHAN, Ibrahim; SAEED, Khalid; KHAN, Idrees. Nanoparticles: Properties, applications and toxicities. *Arabian Journal of Chemistry*, v. 12, n. 7, p. 908–931, 2019. Disponível em: <https://doi.org/10.1016/j.arabjc.2017.05.011>.

KOOTER, Ingeborg *et al.* Molecular Signature of Asthma-Enhanced Sensitivity to CuO Nanoparticle Aerosols from 3D Cell Model. *ACS Nano*, 1 - uso de animais2 - nanoparticula de metal usada em tudo3 - consideramos a hipótese4 - grafico de veen muito legal e explicado5 - descrevendo os resultados por genes6 - genes dependentes da nano7 - Analise de componentem principal para identificar os genes8 - Gene ontologi9 - identificado marcadores para cobre10 - ap, 2019.

KUNZMANN, Andrea *et al.* Toxicology of engineered nanomaterials: Focus on biocompatibility, biodistribution and biodegradation. *Biochimica et Biophysica Acta - General Subjects*, v. 1810, n. 3, p. 361–373, 2011. Disponível em: <http://dx.doi.org/10.1016/j.bbagen.2010.04.007>.

KUSHWAHA, Swatantra Kumar Singh *et al.* Carbon nanotubes as a novel drug delivery system for anticancer therapy: A review. *Brazilian Journal of Pharmaceutical Sciences*, v. 49, n. 4, p. 629–643, 2013.

LI, Tingting *et al. Folate-Functionalized Magnetic-Mesoporous Silica Nanoparticles for Drug/Gene Codelivery to Potentiate the Antitumor Efficacy*. [S.l: s.n.], 2016. v. 8.

LOWE, Rohan *et al.* Transcriptomics technologies. *PLoS Computational Biology*, v. 13, n. 5, p. 1–23, 2017.

MA, Xibo *et al.* Enhanced immunotherapy of SM5-1 in hepatocellular carcinoma by conjugating with gold nanoparticles and its in vivo bioluminescence tomographic evaluation. *Biomaterials*, v. 87, p. 46–56, 2016. Disponível em: <http://dx.doi.org/10.1016/j.biomaterials.2016.02.007>.

MANSON, Eric Naab *et al.* Integrating image fusion with nanoparticle contrast agents for diagnosis: a review. *Egyptian Journal of Radiology and Nuclear Medicine*, v. 51, n. 1, 2020.

MAYNARD, Robert L. Nano-technology and nano-toxicology. *Emerging Health Threats Journal*, v. 5, n. 1, 2012.

MURTHY, Shashi K. Nanoparticles in modern medicine: state of the art and future challenges. *International journal of nanomedicine*, v. 2, n. 2, p. 129–41, 2007. Disponível em: <http://www.ncbi.nlm.nih.gov/pubmed/17722542%0Ahttp://www.pubmedcentral.nih.gov/articlerender.fcgi?artid=PMC2673971>.

OSMOND MCLEOD, Megan J. Surface Coatings Protect against the In vitro Toxicity of Zinc Oxide Nanoparticles in Human Hepatic Stellate Cells. *Journal of Nanomedicine & Nanotechnology*, v. 05, n. 05, 2014.

OSMOND, Megan J.; MCCALL, Maxine J. Zinc oxide nanoparticles in modern sunscreens: An analysis of potential exposure and hazard. *Nanotoxicology*, v.

4, n. 1, p. 15–41, 2010.

PATRA, Jayanta Kumar *et al.* Nano based drug delivery systems: Recent developments and future prospects 10 Technology 1007 Nanotechnology 03 Chemical Sciences 0306 Physical Chemistry (incl. Structural) 03 Chemical Sciences 0303 Macromolecular and Materials Chemistry 11 Medical and He. *Journal of Nanobiotechnology*, v. 16, n. 1, p. 1–33, 2018. Disponível em: <https://doi.org/10.1186/s12951-018-0392-8>.

PAUTLER, Michelle; BRENNER, Sara. Nanomedicine: Promises and challenges for the future of public health. *International Journal of Nanomedicine*, v. 5, n. 1, p. 803–809, 2010.

PISANI, Cédric *et al.* High-throughput, quantitative assessment of the effects of low-dose silica nanoparticles on lung cells: Grasping complex toxicity with a great depth of field. *BMC Genomics*, v. 16, n. 1, p. 1–14, 2015. Disponível em: <???>.

RAI, Mahendra; YADAV, Alka; GADE, Aniket. Silver nanoparticles as a new generation of antimicrobials. *Biotechnology Advances*, v. 27, n. 1, p. 76–83, 2009. Disponível em: <http://dx.doi.org/10.1016/j.biotechadv.2008.09.002>.

RANI, Bibha; SHARMA, V. K. Transcriptome profiling: methods and applications- A review. *Agricultural Reviews*, v. 38, n. 04, 2017.

RUSSELL, WMS; BURCH, RL. *The principles of humane experimental technique*. London: methuen, 1959.

SOTO, Karla; GARZA, K. M.; MURR, L. E. Cytotoxic effects of aggregated nanomaterials. *Acta Biomaterialia*, v. 3, n. 3 SPEC. ISS., p. 351–358, 2007.

SULCZEWSKI, Fernando B *et al.* Nanoparticle vaccines against viral infections. *Archives of virology*, v. 163, n. 9, p. 2313–2325, set. 2018.

TABASUM, Shazia *et al.* Glycoproteins functionalized natural and synthetic polymers for prospective biomedical applications: A review. *INTERNATIONAL JOURNAL OF BIOLOGICAL MACROMOLECULES*, v. 98, p. 748–776, 2017.

THAI, Sheau-Fung *et al.* Differential Genomic Effects of Six Different TiO 2 Nanomaterials on Human Liver HepG2 Cells. *Journal of Biochemical and Molecular Toxicology*, Diferentes tamanhos - diferentes respostasCONCLUSÃO, v. 30, n. 7, p. 331–341, jul. 2016. Disponível em: <http://doi.wiley.com/10.1002/jbt.21798>.

TILTON, Susan C. *et al.* Three human cell types respond to multi-walled carbon nanotubes and titanium dioxide nanobelts with cell-specific transcriptomic and proteomic expression patterns. *Nanotoxicology*, v. 8, n. 5, p. 533–548, 7 ago. 2014. Disponível em: <http://www.tandfonline.com/doi/full/10.3109/17435390.2013.803624>.

TUOMELA, Soile *et al.* Gene Expression Profiling of Immune-Competent Human Cells Exposed to Engineered Zinc Oxide or Titanium Dioxide Nanoparticles. *PLoS ONE*, v. 8, n. 7, 2013.

VAN DER ZANDE, Meike *et al.* Different responses of Caco-2 and MCF-7 cells to silver nanoparticles are based on highly similar mechanisms of action.

Nanotoxicology, v. 10, n. 10, p. 1431–1441, 2016.

VENTOLA, C Lee; BHARALI, Dhruba J; MOUSA, Shaker A. The Nanomedicine Revolution: Part 1: Emerging Concepts. Pharmacy and Therapeutics. *Pharmacology & therapeutics*, v. 128, n. 9, p. 512–525, 2010. Disponível em: <http://www.sciencedirect.com/science/article/pii/S0163725810001506>.

VERMA, Rajni; GANGWAR, Jitendra; SRIVASTAVA, Avanish K. Multiphase TiO2 nanostructures: A review of efficient synthesis, growth mechanism, probing capabilities, and applications in bio-safety and health. *RSC Advances*, v. 7, n. 70, p. 44199–44224, 2017.

WANG, Liying *et al.* Neoplastic-like transformation effect of single-walled and multi-walled carbon nanotubes compared to asbestos on human lung small airway epithelial cells. *Nanotoxicology*, v. 8, n. 5, p. 485–507, 2014.

WANG, Zhong; GERSTEIN, Mark; SNYDER, Michael. RNA-Seq: a revolutionary tool for transcriptomics. *Nature Reviews Genetics*, v. 10, n. 1, p. 57–63, jan. 2009. Disponível em: <http://www.nature.com/articles/nrg2484>.

WOLFRAM, Joy *et al.* Safety of nanoparticles in medicine. *HHS Public Access*, v. 16, n. 1, p. 1671–1681, 2016. Disponível em: <http://dx.doi.org/10.1016/j.expneurol.2016.06.015>.

WU, Bingbing *et al.* Nano genome altas (NGA) of body wide organ responses. *Biomaterials*, v. 205, n. February, p. 38–49, 2019.

ZENG, Yang *et al.* Effects of polyamidoamine dendrimers on a 3-D neurosphere system using human neural progenitor cells. *Toxicological Sciences*, v. 152, n. 1, p. 128–144, 2016.

ZUGAZAGOITIA, Jon *et al.* Current Challenges in Cancer Treatment. *Clinical Therapeutics*, v. 38, n. 7, p. 1551–1566, 2016. Disponível em: <http://dx.doi.org/10.1016/j.clinthera.2016.03.026>.

APPENDICES

SUPLEMENTARY TABLE 1

ID	YEAR	TITLE	SUMMARY	TECHNIQUE	PLATFORM	NUMBER OF SAMPLES	MATERIAL TYPE	MATERIAL STRUCTURE	CELL NAME	CELL TYPE	CELL ORIGIN	ARTICLE	TREATMENT TIME (HOURS)
GSE110410	2019	Microarrays after exposure in Caco-2 cells to titanium dioxide food additive E171 and titanium dioxide nanoparticles and microparticles	Exposure to titanium d	Microarray	Agilent-039494 SurePrint G3 Human GE v2 8x60K Microarray 039381 (Feature Number version)	76	Titaniun	-	Caco-2	Colon adenocarcinoma	Colon	-	2HS+4HS+24hs
GSE138837	2019	Next Generation Sequencing Facilitates Quantitative Analysis of human umbilical vein endothelial cell(HUVEC) with and without treatment of CHIR99021+FGF1	The mortality of patier	RNA-Seq	Illumina NextSeq 500 (Homo sapiens)	2	poly-lactic-co-glycolic acid (PLGA)	-	HUVEC	Human primary umbilical vein endothelial	Umbilical vein endothelial	-	24hs
GSE127773	2019	Molecular signature of asthma-enhanced sensitivity to aerosols of pristine and carboxylated CuO nanoparticles, identified in 3D cell models.	Via extensive compar	RNA-Seq	Agilent-072363 SurePrint G3 Human GE v3 8x60K Microarray 039494 [Probe Name Version]	64	Copper	aerosols	bronchial epithelial	bronchial epithelial	Bronchial	Molecular Signature of Asthma-Enhanced Sensitivity to CuO Nanoparticle Aerosols from 3D Cell Model	24hs
GSE98028	2019	Gene expression changes in Burkitt's lymphoma due to treatment with high density lipoprotein-like nanoparticles (HDL NP)	We report changes in	Microarray	Illumina HumanHT-12 V4.0 expression beadchip	9	Lipid	-	Burkitt's lymphoma	B lymphocytes	Blood	-	48hs
GSE125742	2019	Nano genome altas (NGA) of body wide tissue specific responses	Purpose: In order to d	RNA-Seq	HiSeq X Ten (Homo sapiens)	58	Hydroxyapatite (HANPs)	-	HBMSC	Human bone marrow derived stem cells	Bone marrow	Nano genome altas (NGA) of body wide organ responses.	24hs
GSE127962	2019	Expression data from BEAS-2B cells II	BEAS-2B cells are hu	Microarray	Affymetrix Human Transcriptome Array 2.0	12	Silica	-	bronchial epithelium	bronchial epithelium	Bronchial	-	24hs
GSE121049	2018	Tri-mannose grafting of chitosan nanocarriers remodels the macrophage response to bacterial infection	Background: Infectiou	RNA-Seq	Illumina HiSeq 2500 (Homo sapiens)	18	chitosan	Nanocarrier	Macrophages	Macrophages	Blood	Tri-mannose grafting of chitosan nanocarriers remodels the macrophage response to bacterial infection.	18hs
GSE117056	2018	Differential Genomic Effects of Six Different Nanomaterials on Human Liver HepG2 Cells	Human Hepatocellula	Microarray	Illumina HumanHT-12 V4.0 expression beadchip	120	Cerium	-	HepG2	Liver carcinoma	Liver	Differential Genomic Effects of Six Different TiO2 Nanomaterials on Human Liver HepG2 Cells.	72hs
GSE077355	2018	mRNA expression profile in Al2O3 nanoparticle treated A549 cells	We evaluated the pro	Microarray	Agilent-045997 Arraystar human lncRNA microarray V3 (Probe Name Version)	6	Aluminiun	-	A549	adenocarcinomic human alveolar basal epithelial	Alveolar basal epithelial	Suppression of PTPN6 exacerbates aluminum oxide nanoparticle-induced COPD-like lesions in mice through activation of STAT pathway	168hs
GSE092987	2017	Characterization and molecular mechanistic study of a therapeutic peptide functionalized nanobioconjugate inhibiting the p53-HDM2 interaction in Retinoblastoma	Prepared peptide con	Microarray	Affymetrix Human Gene Expression Array	9	Gold	-	Retinoblastoma	Retinoblastoma	Eye	-	-
GSE092990	2017	Gene expression of magnetic fluid hyperthermia (MFH) in ovarian cancer cells	The expression ovaria	Microarray	Illumina HumanHT-12 V4.0 expression beadchip	6	Iron	Magnetic fluid hyperthermia	HeyA8	adenocarcinoma	Ovarian	HSP70 Inhibition Synergistically Enhances the Effects of Magnetic Fluid Hyperthermia in Ovarian Cancer	0,5hs
GSE098236	2017	Biocompatibility assessment of functionalized magnetic mesoporous silica nanoparticles in human HepaRG cells	We have employed w	Microarray	Agilent-072363 SurePrint G3 Human GE v3 8x60K Microarray 039494 [Feature Number Version]	71	Silica	magnetic mesoporous	HepaRG	Hepatocytes	Liver	Biocompatibility assessment of functionalized magnetic mesoporous silica nanoparticles in human HepaRG cells	24hs+48hs
GSE103101	2017	Increased interleukin-11 and stress genes in human endothelial and human bronchial epithelial cell lines by silver nanoparticles	Because of their sma	Microarray	HuGene-2_0-st] Affymetrix Human Gene 2.0 ST Array [transcript (gene) version]	9	Silver	-	EA.hy926	somatic human umbilical vein endothelial	Umbilical vein endothelial	Increased interleukin-11 and stress genes in human endothelial and human bronchial epithelial cell lines by silver nanoparticles	6hs
GSE092901	2017	Distinct Sets Of Genes Representing Overlapping Biological Functions Are Altered By Intrinsic Properties Of Carbon Nanomaterials In Vitro And In Vivo	This SuperSeries is c	Microarray	Agilent-026652 Whole Human Genome Microarray 4x44K v2 (Feature Number version) Agilent-028005 SurePrint G3 Mouse GE 8x60K Microarray (Feature Number version)	72	carbon	long rigid multiwalled carbon nanotube	THP-1	macrophages	Blood	Network Analysis Reveals Similar Transcriptomic Responses to Intrinsic Properties of Carbon Nanomaterials in Vitro and in Vivo	6hs+24hs
GSE092899	2017	Distinct Sets Of Genes Representing Overlapping Biological Functions Are Altered By Intrinsic Properties Of Carbon Nanomaterials In Vitro And In Vivo [human]	Six different carbon n	Microarray	Agilent-026652 Whole Human Genome Microarray 4x44K v2 (Feature Number version)	48	carbon	long rigid multiwalled carbon nanotube	THP-1	macrophages	Blood	Network Analysis Reveals Similar Transcriptomic Responses to Intrinsic Properties of Carbon Nanomaterials in Vitro and in Vivo	6hs+24hs
GSE089134	2017	Hit-and-run' programing of CAR-T cells using mRNA nanocarriers	RNAseq of ex vivo CD	RNA-Seq	Illumina HiSeq 2500 (Homo sapiens)	14	PBAE447	Nanocarrier	CD 8 T	CD 8 T	Blood	Hit-and-run programming of therapeutic cytoreagents using mRNA nanocarriers.	72hs+192hs
GSE96720	2017	Genome-wide analysis of the toxic effect of hydroxyl-modified Graphene quantum dots (GQD) on normal human esophageal epithelial cells	The objective was to i	Microarray	Agilent-072363 SurePrint G3 Human GE v3 8x60K Microarray 039494 [Probe Name Version]	6	Carbon	Quantum dots	HET-1A	Esophageal epithelial	Esophageal	Hydroxylated-Graphene Quantum Dots Induce DNA Damage and Disrupt Microtubule Structure in Human Esophageal Epithelial Cells	24hs
GSE84982	2016	Different responses of Caco-2 and MCF-7 cells to silver nanoparticles are based on highly similar mechanisms of action	The mode of action o	Microarray	Illumina HumanHT-12 V4.0 expression beadchip	73	Silver	Spherical	Caco-2	Colon adenocarcinoma	Colon	Different responses of Caco-2 and MCF-7 cells to silver nanoparticles are based on highly similar mechanisms of action.	6hs+24hs
GSE82062	2016	Expression data from human lung epithelial cells after amorphous silica nanoparticle exposure for 40 passages	Amorphous silica nan	Microarray	[HTA-2_0] Affymetrix Human Transcriptome Array 2.0 [transcript (gene) version]	6	Silica	Amorphous	Beas-2B	Epithelial	Lung	Amorphous silica nanoparticles induce malignant transformation and tumorigenesis of human lung epithelial cells via P53 signaling	1924hs
GSE69551	2015	Transcriptome study of Caco-2 human intestinal cells following exposure to empty or S-nitrosoglutathione-loaded polymeric nanoparticles	To further study the tr	Microarray	Agilent-039494 SurePrint G3 Human GE v2 8x60K Microarray 039381 (Probe Name version)	16	Poly(ethyl acrylate-co-methyl methacrylate-co-trimethylammonioethyl methacrylate chloride) (PMMAEA)	Polimeric	Caco-2	Colon adenocarcinoma	Colon	-	4hs
GSE62253	2015	Molecular mechanism of silver nanoparticles in human intestinal cell line Caco-2	Silver nanoparticles a	Microarray	HG-U133_Plus_2] Affymetrix Human Genome U133 Plus 2.0 Array	12	Silver	-	Caco-2	Colon adenocarcinoma	Colon	Molecular mechanism of silver nanoparticles in human intestinal cells	24hs

GSE63806	2015	Dose dependent toxicological response of lung cells exposed to silica nanoparticles	We have employed w	Microarray	Agilent-026652 Whole Human Genome Microarray 4x44K v2 (Feature Number version)	38	Silica	-	A549	adenocarcinomic human alveolar basal epithelial	Alveolar basal epithelial	High-throughput, quantitative assessment of the effects of low-dose silica nanoparticles on lung cells: grasping complex toxicity with a great depth of field	24hs+72
GSE65875	2015	Effects of polyamidoamine dendrimer on neuronal differentiation from human neural progenitor cells using the neurosphere assay	Polyamidoamine (PA	Microarray	Agilent-039494 SurePrint G3 Human GE v2 8x60K Microarray 039381 (Probe Name version)	4	polyamidoamine dendrimer (PAMAM)	Dendrimer	hNPCs	neural progenitor	Brain	Effects of Polyamidoamine Dendrimers on a 3-D Neurosphere System Using Human Neural Progenitor Cells.	72hs
GSE55349	2015	Understanding toxicity pathways of gold nanoparticles: RNA expression study on Caco-2 human colon carcinoma cells	A safer design and hi	Microarray	Agilent-028004 SurePrint G3 Human GE 8x60K Microarray (Probe Name Version)	42	Gold	Spherical	Caco-2	Colon adenocarcinoma	Colon	Changes in Caco-2 cells transcriptome profiles upon exposure to gold nanoparticles	24hs+72hs
GSE60128	2014	Toxicity Evaluation of Manufactured CeO2 Nanoparticles Before and After Alteration: Combined Physicochemical and Whole-Genome Expression Analysis in Caco-2 Cells.	We have employed w	Microarray	Agilent-014850 Whole Human Genome Microarray 4x44K G4112F (Feature Number version)	32	Cerium	-	Caco-2	Colon adenocarcinoma	Colon	Toxicity evaluation of manufactured CeO2 nanoparticles before and after alteration: combined physicochemical and whole-genome expression analysis in Caco-2 cells	24hs
GSE60159	2014	Expression data from primary human hepatic stellate cells treated with coated and uncoated ZnO nanoparticles, or ZnSO4	ZnO nanoparticles ca	Microarray	[HG-U133_Plus_2] Affymetrix Human Genome U133 Plus 2.0 Array	12	Zinc	-	hepatic stellate	Hepatic stellate	Liver	Surface Coatings Protect against the In vitro Toxicity of Zinc Oxide Nanoparticles in Human Hepatic Stellate Cells	24hs
GSE59284	2014	SM5-1-conjugated gold nanoparticles for antibody therapy in hepatocellular carcinoma	As a humanized mou	Microarray	[HuGene-1_0-st] Affymetrix Human Gene 1.0 ST Array [transcript (gene) version]	6	Gold	-	HCC-LM3-fLuc	Liver carcinoma	Liver	Enhanced immunotherapy of SM5-1 in hepatocellular carcinoma by conjugating with gold nanoparticles and its in vivobioluminescence tomographic evaluation	24hs
GSE51661	2014	Gene expression profile of human endothelial cells with or without nanoparticles	To understand the the	Microarray	Agilent-014850 Whole Human Genome Microarray 4x44K G4112F (Probe Name version)	9	poly-lactic-co-glycolic acid (PLGA)	Nanocapsules	HUVEC	Human primary umbilical vein endothelial	Umbilical vein endothelial	Inflammatory modulation of stem cells by Magnetic Resonance Imaging (MRI)-detectable nanoparticles.	24hs+168hs
GSE51421	2014	Gene expression profile of hematopoietic stem cells (CD34+ cells) with or without nanoparticles	To understand the the	Microarray	Agilent-014850 Whole Human Genome Microarray 4x44K G4112F (Probe Name version)	12	poly-lactic-co-glycolic acid (PLGA)	Nanocapsules	CD34+	Hematopoietic stem cells	Blood	Inflammatory modulation of stem cells by Magnetic Resonance Imaging (MRI)-detectable nanoparticles.	24hs+168hs
GSE46570	2014	Gene expression analysis of PST-Dox nanoparticles on isolated normal lymphocytes and in cancer cell lines	Analysis of expressior	Microarray	[PrimeView] Affymetrix Human Gene Expression Array	16	galactoxyloglucan polysaccharide (PST-DOX)	Nanocapsules	Lymphocyte	Lymphocyte	Blood	Anticancer activity of galactoxyloglucan polysaccharide–conjugated doxorubicin nanoparticles: mechanistic insights and interactome analysis	24hs
GSE51186	2013	Transcriptome study of THP-1 human monocytes following exposure for 4 h or 24 h to 50 uM S-Nitrosoglutathione, 50 and 200 ug/ml S-Nitrosoglutathione-loaded polymeric and empty Eudragit RL nanoparticles	To further study the tr	Microarray	Agilent-039494 SurePrint G3 Human GE v2 8x60K Microarray 039381 (Feature Number version)	24	Poly(ethyl acrylate-co-methyl methacrylate-co-trimethylammonioethyl methacrylate chloride) (PMMAEA)	Polimeric	THP-1	macrophages	Blood	S-nitrosoglutathione (GSNO) is cytotoxic to intracellular amastigotes and promotes healing of topically treated Leishmania major or Leishmania braziliensis skin lesions	4hs+24hs
GSE45322	2013	Expression data from human olfactory neurosphere derived cells (hONS) established from adult donors treated with coated and uncoated ZnO nanoparticles	ZnO nanoparticles ca	Microarray	[HuGene-1_0-st] Affymetrix Human Gene 1.0 ST Array [transcript (gene) version]	40	Zinc	Rod	hONS	Human Olfactory Mucosa	Nose	Surface coatings of ZnO nanoparticles mitigate differentially a host of transcriptional, protein and signalling responses in primary human olfactory cells	6hs+2hs
GSE45869	2013	Transcriptome study of human mammary epithelial cells following exposure to polymeric Eudragit RS nanoparticles	This SuperSeries is c	Microarray	Agilent-039494 SurePrint G3 Human GE v2 8x60K Microarray 039381 (Feature Number version)	12	Poly(ethyl acrylate-co-methyl methacrylate-co-trimethylammonioethyl methacrylate chloride) (PMMAEA)	Polimeric	HMEC 184	Human mammary	Breast	Unique growth pattern of human mammary epithelial cells induced by polymeric nanoparticles	24hs+48hs+72hs
GSE39330	2013	Nanotoxicogenomic study of ZnO and TiO2 responses (Affymetrix)	A comprehensive in v	Microarray	[HG-U219] Affymetrix Human Genome U219 Array (ENSG Brainarray CDF Version 14.1.0)	71	Zinc	-	HMDM	human monocyte-derived macrophages	Blood	Gene expression profiling of immune-competent human cells exposed to engineered zinc oxide or titanium dioxide nanoparticles.	6hs + 24hs
GSE39316	2013	Nanotoxicogenomic study of ZnO and TiO2 responses (Illumina)	A comprehensive in v	Microarray	Illumina HumanHT-12 V3.0 expression beadchip	90	Zinc	-	HMDM	human monocyte-derived macrophages	Blood	Gene expression profiling of immune-competent human cells exposed to engineered zinc oxide or titanium dioxide nanoparticles	6hs + 24hs
GSE41178	2013	Whole genome profile of SWNCT and MWCNT vs. asbestos subchronic exposures to human small airway epithelial cells	Recent in vivo studies	Microarray	NimbleGen Homo sapiens Expression Array [100718_HG18_opt_expr]	18	Carbon	Single wall	SAEC-hTERT	small airway epithelial cells	Lung	Neoplastic-like transformation effect of single-walled and multi-walled carbon nanotubes compared to asbestos on human lung small airway epithelial cells	4320hs
GSE43515	2013	Effect of MWCNT on Lung Fibroblast gene expression	Multi-walled carbon n	Microarray	[HG-U133A_2] Affymetrix Human Genome U133A 2.0 Array	54	Carbon	Carbon Black	16lu	fibroblasts	Lung	-	4 + 24 + 48hs
GSE42068	2012	Three human cell types respond to multi-walled carbon nanotubes and titanium dioxide nanobelts with cell-specific transcriptomic and proteomic expression [THP-1 cells]	To identify key biologi	Microarray	[HG-U133A_2] Affymetrix Human Genome U133A 2.0 Array	30	Carbon	Multi wall	THP-1	macrophages	Blood	Three human cell types respond to multi-walled carbon nanotubes and titanium dioxide nanobelts with cell-specific transcriptomic and proteomic expression patterns	1 + 24hs
GSE42067	2012	Three human cell types respond to multi-walled carbon nanotubes and titanium dioxide nanobelts with cell-specific transcriptomic and proteomic expression [THP-1 cells]	To identify key biologi	Microarray	[HG-U133A_2] Affymetrix Human Genome U133A 2.0 Array	30	Carbon	Multi wall	SAE	small airway epithelial cells	Lung	Three human cell types respond to multi-walled carbon nanotubes and titanium dioxide nanobelts with cell-specific transcriptomic and proteomic expression patterns	1 + 24hs
GSE42066	2012	Three human cell types respond to multi-walled carbon nanotubes and titanium dioxide nanobelts with cell-specific transcriptomic and proteomic expression [THP-1 cells]	To identify key biologi	Microarray	[HG-U133A_2] Affymetrix Human Genome U133A 2.0 Array	30	Carbon	Multi wall	Caco-2	Colon adenocarcinoma	Colon	Three human cell types respond to multi-walled carbon nanotubes and titanium dioxide nanobelts with cell-specific transcriptomic and proteomic expression patterns	1 + 24hs

GSE20431	2011	Gene expression profiling on FePro labeled bone marrow stromal cells	Superparamagnetic ir	Microarray	CCDTM Hs_CCDTM36k - version 1 (derived from GPL7088)	15	Gold	-	HBMSC	Human bone marrow derived stem cells	Bone marrow	Superparamagnetic iron oxide nanoparticles labeling of bone marrow stromal (mesenchymal) cells does not affect their "stemness"	64hs
GSE15248	2010	Biocompatibility and Discovery of the Potential Applications of Magnetite (Fe3O4) Nanoparticles	A Transcriptomics Ap	Microarray	Illumina human-6 v2.0 expression beadchip	6	Iron	Nanocrystals	HeLa	Human cervix epitheloid carcinoma	Cervix	Magnetite (Fe3O4) nanocrystals affect the expression of genes involved in the TGF-beta signalling pathway	12hs
GSE20692	2010	mRNA and microRNA microarray analysis on human Jurkat T cells exposed to silver nanoparticles and silver ions	To identify genes and	Microarray	Illumina HumanRef-8 v3.0 expression beadchip	12	Silver	-	Jurkat	T cell leukemia	Blood	Integrated mRNA and micro RNA profiling reveals epigenetic mechanism of differential sensitivity of Jurkat T cells to AgNPs and Ag ions	24hs
GSE14452	2009	DNA microarray analyses for HepG2 cells exposed to silver nanoparticles	From the result of the	Microarray	[HG-Focus] Affymetrix Human HG-Focus Target Array	15	Silver	-	HepG2	Liver carcinoma	Liver	In Vitro Toxicity of Silver Nanoparticles at Noncytotoxic Doses to HepG2 Human Hepatoma Cells	24hs+48hs
GSE3364	2005	Fullerene treatment of HUVECs	Control untreated ver	Microarray	[HG-U133_Plus_2] Affymetrix Human Genome U133 Plus 2.0 Array	4	carbon	Fullerene	HUVEC	Human primary umbilical vein endothelial	Umbilical vein endothelial	Cytotoxicity of water-soluble fullerene in vascular endothelial cells	24hs

Suplemmentary Table 2

Suplemmentary Table 2: List of downregulated and upregulated DEGs identified by integrative Carbon

Dataset	Cell type	Morphology	Size	Downregulated shared genes
GSE43515	16LU	Carbon Black	-	MTSS1
GSE43515	16LU	MultiWalled Carbon	-	
GSE96720	HET1A	Quantun DOTS	4-6nm	
GSE43515	16LU	Carbon Black	-	KDM6B
GSE43515	16LU	MultiWalled Carbon	-	
GSE42067	SAE	MultiWalled Carbon	5-10x20-30nm	
GSE43515	16LU	Carbon Black	-	NINL NR4A2 CDC25B DDB2 PDGFRB SVIL CHKB-CPT1B///CPT1B NAV2 RRAGC
GSE43515	16LU	MultiWalled Carbon	-	
GSE43515	16LU	Carbon Black	-	N4BP2L2
GSE42067	SAE	MultiWalled Carbon	5-10x20-30nm	
GSE43515	16LU	MultiWalled Carbon	-	TNS1
GSE42067	SAE	MultiWalled Carbon	5-10x20-30nm	
GSE42066	CACO2	MultiWalled Carbon	5-10x20-30nm	PTGER3 AAK1
GSE3364	HUVEC	Fulrene	4,7-9,5nm	
GSE42066	CACO2	MultiWalled Carbon	5-10x20-30nm	CD44 QPCT
GSE42068	THP1	MultiWalled Carbon	5-10x20-30nm	
GSE3364	HUVEC	Fulrene	4,7-9,5nm	MMP8 TRAF1
GSE42068	THP1	MultiWalled Carbon	5-10x20-30nm	
Dataset	**Cell type**	**Morphology**	**Size**	**Upregulated shared genes**
GSE43515	16LU	Carbon Black	-	NQO1 IGFBP5
GSE43515	16LU	MultiWalled Carbon	-	
GSE42067	SAE	MultiWalled Carbon	5-10x20-30nm	
GSE43515	16LU	Carbon Black	-	DPP4

GSE42067	SAE	MultiWalled Carbon	5-10x20-30nm	DPP4
GSE43515	16LU	Carbon Black	-	RAB14
GSE42066	CACO2	MultiWalled Carbon	5-10x20-30nm	
GSE43515	16LU	Carbon Black	-	DUSP6 PAPSS2 SLC16A7 SRPRA ATP1B1 TRAK2
GSE43515	16LU	MultiWalled Carbon	-	SLC1A1 RIOK2 BDKRB1 ARHGAP29 RASSF2 EDNRA
GSE42067	SAE	MultiWalled Carbon	5-10x20-30nm	LBH
GSE42068	THP1	MultiWalled Carbon	5-10x20-30nm	
GSE42066	CACO2	MultiWalled Carbon	5-10x20-30nm	DDX17
GSE42068	THP1	MultiWalled Carbon	5-10x20-30nm	
GSE3364	HUVEC	Fulrene	4,7-9,5nm	CSRNP3
GSE42067	SAE	MultiWalled Carbon	5-10x20-30nm	
GSE96720	HET1A	Quantun DOTS	4-6nm	ABHD5 NEDD9 TRIB1
GSE42067	SAE	MultiWalled Carbon	5-10x20-30nm	
GSE42066	CACO2	MultiWalled Carbon	5-10x20-30nm	CEP350 TRIB2
GSE42067	SAE	MultiWalled Carbon	5-10x20-30nm	
GSE42066	CACO2	MultiWalled Carbon	5-10x20-30nm	CCR2
GSE3364	HUVEC	Fulrene	4,7-9,5nm	
GSE42066	CACO2	MultiWalled Carbon	5-10x20-30nm	EGR1 NOP14-AS1 SCAF11
GSE96720	HET1A	Quantun DOTS	4-6nm	
GSE43515	16LU	MultiWalled Carbon	-	CITED2 TPM4 UBE2H
GSE96720	HET1A	Quantun DOTS	4-6nm	
GSE43515	16LU	MultiWalled Carbon	-	MARCKS MTMR1 PRKCI SYNJ2BP-COX16///SYNJ2BP CALD1 RYBP
GSE42066	CACO2	MultiWalled Carbon	5-10x20-30nm	

Gold

Dataset	Cell type	Morphology	Size	Downregulated shared genes
GSE55349	CACO2	Spherical	40nm	CYP1A1
GSE55349	CACO2	Spherical	5nm	
GSE55349	CACO2	Spherical	40nm	LAMC2 TXNIP

GSE59284	HCC-LM3	Spherical	5nm	LAMC2 TXNIP

Dataset	Cell type	Morphology	Size	Upregulated shared genes
GSE55349	CACO2	Spherical	40nm	UBD
GSE55349	CACO2	Spherical	5nm	
GSE59284	HCC-LM3	Spherical	5nm	
GSE55349	CACO2	Spherical	40nm	C6orf162 ARL1
GSE55349	CACO2	Spherical	5nm	LOC100128869 DSTNP2

Silver

Dataset	Cell type	Morphology	Size	Downregulated shared genes
GSE84982	CACO2	Spherical	110nm	MT1H MT2A
GSE84982	CACO2	Spherical	20nm	
GSE62253	CACO2	Spherical	15-28nm	
GSE84982	CACO2	Spherical	30nm	
GSE84982	CACO2	Spherical	60nm	
GSE14452	HEPG2	-	7-10nm	
GSE20692	JURKAT	-	<100nm	
GSE84982	MCF7	Spherical	110nm	
GSE84982	MCF7	Spherical	20nm	
GSE84982	MCF7	Spherical	30nm	
GSE84982	MCF7	Spherical	60nm	
GSE84982	CACO2	Spherical	110nm	FHL2 MT1X
GSE84982	CACO2	Spherical	20nm	
GSE62253	CACO2	Spherical	15-28nm	
GSE84982	CACO2	Spherical	30nm	
GSE84982	CACO2	Spherical	60nm	
GSE14452	HEPG2	-	7-10nm	
GSE84982	MCF7	Spherical	110nm	
GSE84982	MCF7	Spherical	20nm	
GSE84982	MCF7	Spherical	30nm	
GSE84982	MCF7	Spherical	60nm	
GSE84982	CACO2	Spherical	110nm	MT1E MT1G MT1F
GSE84982	CACO2	Spherical	20nm	
GSE62253	CACO2	Spherical	15-28nm	
GSE84982	CACO2	Spherical	30nm	
GSE84982	CACO2	Spherical	60nm	
GSE20692	JURKAT	-	<100nm	
GSE84982	MCF7	Spherical	110nm	
GSE84982	MCF7	Spherical	20nm	
GSE84982	MCF7	Spherical	30nm	
GSE84982	MCF7	Spherical	60nm	
GSE84982	CACO2	Spherical	110nm	PPP1R15A
GSE84982	CACO2	Spherical	20nm	
GSE62253	CACO2	Spherical	15-28nm	
GSE84982	CACO2	Spherical	30nm	
GSE84982	CACO2	Spherical	60nm	
GSE20692	JURKAT	-	<100nm	
GSE84982	MCF7	Spherical	20nm	

GSE84982	MCF7	Spherical	30nm	
GSE84982	MCF7	Spherical	60nm	
GSE84982	CACO2	Spherical	110nm	
GSE84982	CACO2	Spherical	20nm	
GSE62253	CACO2	Spherical	15-28nm	
GSE84982	CACO2	Spherical	30nm	HMOX1 SRXN1 GCLM
GSE84982	CACO2	Spherical	60nm	TXNRD1 SLC30A1 HSPA6
GSE84982	MCF7	Spherical	110nm	DUSP1 VGF SLC7A11
GSE84982	MCF7	Spherical	20nm	
GSE84982	MCF7	Spherical	30nm	
GSE84982	MCF7	Spherical	60nm	
GSE84982	CACO2	Spherical	110nm	
GSE84982	CACO2	Spherical	20nm	
GSE84982	CACO2	Spherical	30nm	
GSE84982	CACO2	Spherical	60nm	
GSE20692	JURKAT	-	<100nm	IDS MT1A
GSE84982	MCF7	Spherical	110nm	
GSE84982	MCF7	Spherical	20nm	
GSE84982	MCF7	Spherical	30nm	
GSE84982	MCF7	Spherical	60nm	
GSE84982	CACO2	Spherical	110nm	
GSE84982	CACO2	Spherical	20nm	
GSE62253	CACO2	Spherical	15-28nm	
GSE84982	CACO2	Spherical	30nm	CRYAB
GSE84982	CACO2	Spherical	60nm	
GSE84982	MCF7	Spherical	20nm	
GSE84982	MCF7	Spherical	30nm	
GSE84982	MCF7	Spherical	60nm	
GSE84982	CACO2	Spherical	110nm	
GSE84982	CACO2	Spherical	20nm	MT1B SEL1L3 TEX19 PTGR1
GSE84982	CACO2	Spherical	30nm	DUSP5 ULBP2 G6PD PLD1
GSE84982	CACO2	Spherical	60nm	AKR1C2 AKR1C4 ADM
GSE84982	MCF7	Spherical	110nm	HSPA1A GPX2 ERRFI1
GSE84982	MCF7	Spherical	20nm	MLLT11 CLCF1
GSE84982	MCF7	Spherical	30nm	
GSE84982	MCF7	Spherical	60nm	
GSE84982	CACO2	Spherical	20nm	
GSE62253	CACO2	Spherical	15-28nm	
GSE84982	CACO2	Spherical	30nm	
GSE84982	CACO2	Spherical	60nm	EGR1
GSE84982	MCF7	Spherical	110nm	
GSE84982	MCF7	Spherical	20nm	
GSE84982	MCF7	Spherical	30nm	
GSE84982	MCF7	Spherical	60nm	
GSE84982	CACO2	Spherical	110nm	
GSE84982	CACO2	Spherical	20nm	
GSE62253	CACO2	Spherical	15-28nm	
GSE84982	CACO2	Spherical	30nm	HSPH1
GSE84982	CACO2	Spherical	60nm	
GSE14452	HEPG2	-	7-10nm	

GSE84982	MCF7	Spherical	20nm	
GSE84982	CACO2	Spherical	110nm	
GSE84982	CACO2	Spherical	20nm	
GSE62253	CACO2	Spherical	15-28nm	
GSE84982	CACO2	Spherical	30nm	UCHL1
GSE84982	CACO2	Spherical	60nm	
GSE84982	MCF7	Spherical	20nm	
GSE84982	MCF7	Spherical	30nm	
GSE84982	CACO2	Spherical	110nm	
GSE84982	CACO2	Spherical	20nm	
GSE62253	CACO2	Spherical	15-28nm	
GSE84982	CACO2	Spherical	30nm	ZFAND2A
GSE84982	CACO2	Spherical	60nm	
GSE84982	MCF7	Spherical	20nm	
GSE84982	MCF7	Spherical	60nm	
GSE84982	CACO2	Spherical	110nm	
GSE84982	CACO2	Spherical	20nm	
GSE62253	CACO2	Spherical	15-28nm	
GSE84982	CACO2	Spherical	30nm	MYADM
GSE84982	CACO2	Spherical	60nm	
GSE84982	MCF7	Spherical	110nm	
GSE84982	MCF7	Spherical	60nm	
GSE84982	CACO2	Spherical	110nm	
GSE84982	CACO2	Spherical	20nm	
GSE84982	CACO2	Spherical	30nm	
GSE84982	CACO2	Spherical	60nm	S100P SQSTM1 SNORD33
GSE84982	MCF7	Spherical	20nm	
GSE84982	MCF7	Spherical	30nm	
GSE84982	MCF7	Spherical	60nm	
GSE84982	CACO2	Spherical	110nm	
GSE84982	CACO2	Spherical	20nm	
GSE84982	CACO2	Spherical	30nm	
GSE84982	CACO2	Spherical	60nm	GPAT3
GSE84982	MCF7	Spherical	110nm	
GSE84982	MCF7	Spherical	30nm	
GSE84982	MCF7	Spherical	60nm	
GSE84982	CACO2	Spherical	110nm	
GSE84982	CACO2	Spherical	30nm	
GSE84982	CACO2	Spherical	60nm	
GSE84982	MCF7	Spherical	110nm	AKR1B10
GSE84982	MCF7	Spherical	20nm	
GSE84982	MCF7	Spherical	30nm	
GSE84982	MCF7	Spherical	60nm	
GSE84982	CACO2	Spherical	20nm	
GSE84982	CACO2	Spherical	30nm	
GSE84982	CACO2	Spherical	60nm	
GSE84982	MCF7	Spherical	110nm	PELO BHLHE40 ZYX TCF7 KAT5
GSE84982	MCF7	Spherical	20nm	
GSE84982	MCF7	Spherical	30nm	
GSE84982	MCF7	Spherical	60nm	

GSE84982	CACO2	Spherical	30nm	
GSE84982	CACO2	Spherical	60nm	
GSE20692	JURKAT	-	<100nm	
GSE84982	MCF7	Spherical	110nm	NQO1
GSE84982	MCF7	Spherical	20nm	
GSE84982	MCF7	Spherical	30nm	
GSE84982	MCF7	Spherical	60nm	
GSE84982	CACO2	Spherical	110nm	
GSE84982	CACO2	Spherical	20nm	
GSE62253	CACO2	Spherical	15-28nm	SERPINE2 PHLDA2 FOSL1
GSE84982	CACO2	Spherical	30nm	
GSE84982	CACO2	Spherical	60nm	
GSE14452	HEPG2	-	7-10nm	
GSE84982	CACO2	Spherical	110nm	
GSE84982	CACO2	Spherical	20nm	
GSE62253	CACO2	Spherical	15-28nm	ATF3
GSE84982	CACO2	Spherical	30nm	
GSE84982	CACO2	Spherical	60nm	
GSE20692	JURKAT	-	<100nm	
GSE84982	CACO2	Spherical	110nm	
GSE84982	CACO2	Spherical	20nm	
GSE84982	CACO2	Spherical	30nm	CTGF
GSE84982	CACO2	Spherical	60nm	
GSE84982	MCF7	Spherical	20nm	
GSE84982	MCF7	Spherical	30nm	
GSE84982	CACO2	Spherical	110nm	
GSE84982	CACO2	Spherical	20nm	
GSE84982	CACO2	Spherical	30nm	IER3
GSE84982	CACO2	Spherical	60nm	
GSE84982	MCF7	Spherical	30nm	
GSE84982	MCF7	Spherical	60nm	
GSE84982	CACO2	Spherical	110nm	
GSE84982	CACO2	Spherical	20nm	
GSE84982	CACO2	Spherical	30nm	CSRP1
GSE84982	CACO2	Spherical	60nm	
GSE84982	MCF7	Spherical	110nm	
GSE84982	MCF7	Spherical	60nm	
GSE84982	CACO2	Spherical	20nm	
GSE84982	CACO2	Spherical	30nm	
GSE84982	CACO2	Spherical	60nm	TRIB1
GSE84982	MCF7	Spherical	110nm	
GSE84982	MCF7	Spherical	30nm	
GSE84982	MCF7	Spherical	60nm	
GSE84982	CACO2	Spherical	20nm	
GSE84982	CACO2	Spherical	30nm	
GSE84982	MCF7	Spherical	110nm	SNORA10
GSE84982	MCF7	Spherical	20nm	
GSE84982	MCF7	Spherical	30nm	
GSE84982	MCF7	Spherical	60nm	
GSE84982	CACO2	Spherical	20nm	

GSE84982	CACO2	Spherical	60nm	
GSE84982	MCF7	Spherical	110nm	AKR1C3
GSE84982	MCF7	Spherical	20nm	
GSE84982	MCF7	Spherical	30nm	
GSE84982	MCF7	Spherical	60nm	
GSE84982	CACO2	Spherical	30nm	
GSE84982	CACO2	Spherical	60nm	
GSE84982	MCF7	Spherical	110nm	PANX2 RND3
GSE84982	MCF7	Spherical	20nm	
GSE84982	MCF7	Spherical	30nm	
GSE84982	MCF7	Spherical	60nm	
GSE84982	CACO2	Spherical	110nm	DNAJB1 NPPB RAB3B FOS
GSE84982	CACO2	Spherical	20nm	SOX8 GLA MT1M CXCL8
GSE62253	CACO2	Spherical	15-28nm	MAFB ZCCHC12 MAP1LC3B
GSE84982	CACO2	Spherical	30nm	BAG3 C11orf96 CCK TUBB3
GSE84982	CACO2	Spherical	60nm	JUN SLC30A2 MAFF
GSE84982	CACO2	Spherical	110nm	
GSE84982	CACO2	Spherical	20nm	
GSE84982	CACO2	Spherical	30nm	CYR61
GSE84982	CACO2	Spherical	60nm	
GSE14452	HEPG2	-	7-10nm	
GSE84982	CACO2	Spherical	110nm	
GSE84982	CACO2	Spherical	20nm	GADD45G SNORD14C
GSE84982	CACO2	Spherical	30nm	HSPA1B FOSB GABARAPL1
GSE84982	CACO2	Spherical	60nm	RIOK3 SAT1 UBC
GSE84982	MCF7	Spherical	20nm	
GSE84982	CACO2	Spherical	110nm	
GSE84982	CACO2	Spherical	20nm	
GSE84982	CACO2	Spherical	30nm	PFKP
GSE84982	CACO2	Spherical	60nm	
GSE84982	MCF7	Spherical	60nm	
GSE84982	CACO2	Spherical	110nm	
GSE84982	CACO2	Spherical	30nm	
GSE84982	CACO2	Spherical	60nm	CT45A3
GSE84982	MCF7	Spherical	20nm	
GSE84982	MCF7	Spherical	30nm	
GSE84982	CACO2	Spherical	20nm	
GSE84982	CACO2	Spherical	30nm	
GSE84982	CACO2	Spherical	60nm	NUDT1
GSE84982	MCF7	Spherical	110nm	
GSE84982	MCF7	Spherical	60nm	
GSE84982	CACO2	Spherical	20nm	
GSE84982	CACO2	Spherical	30nm	
GSE20692	JURKAT	-	<100nm	DDIT3
GSE84982	MCF7	Spherical	110nm	
GSE84982	MCF7	Spherical	60nm	
GSE84982	CACO2	Spherical	20nm	
GSE20692	JURKAT	-	<100nm	
GSE84982	MCF7	Spherical	110nm	TRIB3
GSE84982	MCF7	Spherical	30nm	

GSE84982	MCF7	Spherical	60nm	
GSE84982	CACO2	Spherical	20nm	
GSE84982	MCF7	Spherical	110nm	
GSE84982	MCF7	Spherical	20nm	GDF15
GSE84982	MCF7	Spherical	30nm	
GSE84982	MCF7	Spherical	60nm	
GSE62253	CACO2	Spherical	15-28nm	
GSE84982	MCF7	Spherical	110nm	
GSE84982	MCF7	Spherical	20nm	SLC7A5
GSE84982	MCF7	Spherical	30nm	
GSE84982	MCF7	Spherical	60nm	
GSE84982	CACO2	Spherical	30nm	
GSE84982	CACO2	Spherical	60nm	
GSE84982	MCF7	Spherical	110nm	PIR
GSE84982	MCF7	Spherical	30nm	
GSE84982	MCF7	Spherical	60nm	
GSE84982	CACO2	Spherical	60nm	
GSE84982	MCF7	Spherical	110nm	
GSE84982	MCF7	Spherical	20nm	CBR3 UGT1A6
GSE84982	MCF7	Spherical	30nm	
GSE84982	MCF7	Spherical	60nm	
GSE14452	HEPG2	-	7-10nm	
GSE84982	MCF7	Spherical	110nm	
GSE84982	MCF7	Spherical	20nm	ABCC3
GSE84982	MCF7	Spherical	30nm	
GSE84982	MCF7	Spherical	60nm	
GSE20692	JURKAT	-	<100nm	
GSE84982	MCF7	Spherical	110nm	
GSE84982	MCF7	Spherical	20nm	FTH1P3
GSE84982	MCF7	Spherical	30nm	
GSE84982	MCF7	Spherical	60nm	
GSE84982	CACO2	Spherical	110nm	RN7SK EDN1 ANXA1 FHL3
GSE84982	CACO2	Spherical	20nm	CEACAM6 CRABP2 CRYBA4
GSE84982	CACO2	Spherical	30nm	SLC16A3 IER5 HIST2H2AA3
GSE84982	CACO2	Spherical	60nm	SNORD14D KLF6 EMP1
GSE84982	CACO2	Spherical	110nm	
GSE84982	CACO2	Spherical	30nm	GSR TTC1
GSE84982	CACO2	Spherical	60nm	
GSE84982	MCF7	Spherical	110nm	
GSE84982	CACO2	Spherical	20nm	
GSE62253	CACO2	Spherical	15-28nm	RGS2 EPHA2 PEA15 MCL1
GSE84982	CACO2	Spherical	30nm	
GSE84982	CACO2	Spherical	60nm	
GSE84982	CACO2	Spherical	20nm	
GSE62253	CACO2	Spherical	15-28nm	IL11
GSE84982	CACO2	Spherical	60nm	
GSE84982	MCF7	Spherical	20nm	
GSE84982	CACO2	Spherical	20nm	
GSE84982	CACO2	Spherical	30nm	GPRC5A
GSE84982	CACO2	Spherical	60nm	

GSE14452	HEPG2	-	7-10nm	
GSE84982	CACO2	Spherical	20nm	HSPA7
GSE84982	CACO2	Spherical	30nm	
GSE84982	CACO2	Spherical	60nm	
GSE84982	MCF7	Spherical	20nm	
GSE84982	CACO2	Spherical	20nm	IFRD1
GSE84982	CACO2	Spherical	30nm	
GSE84982	CACO2	Spherical	60nm	
GSE84982	MCF7	Spherical	110nm	
GSE84982	CACO2	Spherical	20nm	ABHD4
GSE84982	CACO2	Spherical	60nm	
GSE84982	MCF7	Spherical	20nm	
GSE84982	MCF7	Spherical	60nm	
GSE62253	CACO2	Spherical	15-28nm	PALLD
GSE84982	MCF7	Spherical	110nm	
GSE84982	MCF7	Spherical	30nm	
GSE84982	MCF7	Spherical	60nm	
GSE84982	CACO2	Spherical	60nm	SNAR-A1
GSE84982	MCF7	Spherical	20nm	
GSE84982	MCF7	Spherical	30nm	
GSE84982	MCF7	Spherical	60nm	
GSE14452	HEPG2	-	7-10nm	TALDO1
GSE84982	MCF7	Spherical	110nm	
GSE84982	MCF7	Spherical	20nm	
GSE84982	MCF7	Spherical	60nm	
GSE20692	JURKAT	-	<100nm	PSAT1 ASS1 ASNS
GSE84982	MCF7	Spherical	110nm	
GSE84982	MCF7	Spherical	30nm	
GSE84982	MCF7	Spherical	60nm	
GSE84982	MCF7	Spherical	110nm	TKT MPZL2 P4HA2 NAMPT
GSE84982	MCF7	Spherical	20nm	FAM105A TSKU LRP8
GSE84982	MCF7	Spherical	30nm	TNFRSF21 CTSL SLC3A2
GSE84982	MCF7	Spherical	60nm	RASD1 MGST1 BNIP3 FTH1
GSE84982	CACO2	Spherical	110nm	RNU6-1 PIM1 DEFB103A
GSE84982	CACO2	Spherical	20nm	CLTB
GSE84982	CACO2	Spherical	30nm	
GSE84982	CACO2	Spherical	110nm	PDLIM5
GSE84982	CACO2	Spherical	20nm	
GSE84982	CACO2	Spherical	60nm	
GSE84982	CACO2	Spherical	110nm	ZNF114
GSE62253	CACO2	Spherical	15-28nm	
GSE84982	CACO2	Spherical	60nm	
GSE84982	CACO2	Spherical	110nm	ACTA1 ATP6V1E1 DYNC2H1
GSE84982	CACO2	Spherical	30nm	ZNF280A
GSE84982	CACO2	Spherical	60nm	
GSE84982	CACO2	Spherical	110nm	SNORA14B
GSE84982	MCF7	Spherical	20nm	
GSE84982	MCF7	Spherical	30nm	
GSE84982	CACO2	Spherical	20nm	HSPB8 DDIT4 ARL14
GSE84982	CACO2	Spherical	30nm	GADD45A YRDC TNFAIP8

GSE84982	CACO2	Spherical	60nm	FLNC FKBP4 RNF24 FGF19
GSE84982	CACO2	Spherical	30nm	
GSE84982	CACO2	Spherical	60nm	FSCN1
GSE14452	HEPG2	-	7-10nm	
GSE84982	CACO2	Spherical	60nm	
GSE14452	HEPG2	-	7-10nm	SFN
GSE84982	MCF7	Spherical	110nm	
GSE84982	CACO2	Spherical	60nm	
GSE84982	MCF7	Spherical	20nm	PSMC4
GSE84982	MCF7	Spherical	30nm	
GSE14452	HEPG2	-	7-10nm	
GSE84982	MCF7	Spherical	20nm	PSMD1 NME1
GSE84982	MCF7	Spherical	60nm	
GSE14452	HEPG2	-	7-10nm	
GSE84982	MCF7	Spherical	30nm	DTNA
GSE84982	MCF7	Spherical	60nm	
GSE20692	JURKAT	-	<100nm	
GSE84982	MCF7	Spherical	30nm	FTL PHGDH
GSE84982	MCF7	Spherical	60nm	
GSE20692	JURKAT	-	<100nm	
GSE84982	MCF7	Spherical	110nm	PCK2
GSE84982	MCF7	Spherical	60nm	
GSE84982	MCF7	Spherical	20nm	ANGPTL4 SCPEP1 NDRG1
GSE84982	MCF7	Spherical	30nm	MUCL1 CCL26 CENPV
GSE84982	MCF7	Spherical	60nm	TREML3P GPX3 SHC4
GSE84982	MCF7	Spherical	110nm	
GSE84982	MCF7	Spherical	20nm	DNAJC3 UPP1
GSE84982	MCF7	Spherical	30nm	
GSE84982	MCF7	Spherical	110nm	
GSE84982	MCF7	Spherical	20nm	PKM
GSE84982	MCF7	Spherical	60nm	
GSE84982	MCF7	Spherical	110nm	DFFB NRP1 B4GALNT1 BRI3
GSE84982	MCF7	Spherical	30nm	HTATIP2 NAA20 KLF2 ITGAV
GSE84982	MCF7	Spherical	60nm	CLDN1 IER5L PPP2R2C
GSE84982	CACO2	Spherical	110nm	UTP11
GSE84982	CACO2	Spherical	20nm	
GSE84982	CACO2	Spherical	110nm	ATP6V1D
GSE84982	CACO2	Spherical	30nm	
GSE84982	CACO2	Spherical	110nm	DLL1
GSE84982	CACO2	Spherical	60nm	
GSE84982	CACO2	Spherical	110nm	EMC3
GSE14452	HEPG2	-	7-10nm	
GSE84982	CACO2	Spherical	110nm	RIT1
GSE84982	MCF7	Spherical	20nm	
GSE84982	CACO2	Spherical	20nm	RRAD
GSE62253	CACO2	Spherical	15-28nm	
GSE84982	CACO2	Spherical	20nm	SLC25A25 VCX3B
GSE84982	CACO2	Spherical	30nm	TNFRSF10B TM4SF1 LDLR
GSE84982	CACO2	Spherical	20nm	HSPB1 BIK NECAB3 LMCD1
GSE84982	CACO2	Spherical	60nm	GEM CCND3

GSE62253	CACO2	Spherical	15-28nm	MRTO4
GSE14452	HEPG2	-	7-10nm	
GSE62253	CACO2	Spherical	15-28nm	ARC
GSE84982	MCF7	Spherical	20nm	
GSE84982	CACO2	Spherical	30nm	TAX1BP1 SNORD15B MICB
GSE84982	CACO2	Spherical	60nm	SLC20A1 ZFAND5 HOXB8
GSE84982	CACO2	Spherical	30nm	DLC1
GSE14452	HEPG2	-	7-10nm	
GSE84982	CACO2	Spherical	60nm	CSRP2
GSE14452	HEPG2	-	7-10nm	
GSE14452	HEPG2	-	7-10nm	ADD3 UBE2C CCNB2
GSE20692	JURKAT	-	<100nm	SEC14L1 STAT1
GSE14452	HEPG2	-	7-10nm	CAPN2
GSE84982	MCF7	Spherical	60nm	
GSE14452	HEPG2	-	7-10nm	DSTN PSMD2 ITGAE S100A11
GSE84982	MCF7	Spherical	110nm	
GSE20692	JURKAT	-	<100nm	GPT2
GSE84982	MCF7	Spherical	60nm	
GSE84982	MCF7	Spherical	20nm	TUBA4A HLA-H DHRS3
GSE84982	MCF7	Spherical	30nm	
GSE84982	MCF7	Spherical	20nm	MSRB1 DNAJA4 HPCAL1
GSE84982	MCF7	Spherical	60nm	RRAGD
GSE84982	MCF7	Spherical	110nm	KLK6 ENO2
GSE84982	MCF7	Spherical	20nm	
GSE84982	MCF7	Spherical	30nm	PHLDA1 WWC3 NABP1
GSE84982	MCF7	Spherical	60nm	PLOD3 MMP9
GSE84982	MCF7	Spherical	110nm	PAWR BCYRN1 GAL S100A9
GSE84982	MCF7	Spherical	30nm	
GSE84982	MCF7	Spherical	110nm	LYPD6B STX3 C20orf24 SHC1
GSE84982	MCF7	Spherical	60nm	PDLIM7 CIDECP DPH3

Dataset	**Cell type**	**Morphology**	**Size**	**Upregulated shared genes**
GSE84982	CACO2	Spherical	20nm	ENSA MED8
GSE84982	CACO2	Spherical	30nm	
GSE84982	CACO2	Spherical	60nm	
GSE84982	MCF7	Spherical	110nm	
GSE84982	MCF7	Spherical	20nm	
GSE84982	MCF7	Spherical	30nm	
GSE84982	MCF7	Spherical	60nm	
GSE84982	CACO2	Spherical	110nm	HIST1H2BD
GSE84982	CACO2	Spherical	20nm	
GSE84982	CACO2	Spherical	30nm	
GSE84982	CACO2	Spherical	60nm	
GSE20692	JURKAT	-	<100nm	
GSE84982	MCF7	Spherical	20nm	
GSE84982	MCF7	Spherical	30nm	
GSE84982	CACO2	Spherical	110nm	MXD3
GSE84982	CACO2	Spherical	30nm	
GSE84982	CACO2	Spherical	60nm	
GSE84982	MCF7	Spherical	20nm	

GSE84982	MCF7	Spherical	30nm	
GSE84982	CACO2	Spherical	110nm	CTDSP1
GSE84982	CACO2	Spherical	20nm	
GSE84982	CACO2	Spherical	30nm	
GSE84982	CACO2	Spherical	60nm	
GSE84982	MCF7	Spherical	30nm	
GSE84982	MCF7	Spherical	110nm	MSMB
GSE84982	MCF7	Spherical	20nm	
GSE84982	MCF7	Spherical	30nm	
GSE84982	MCF7	Spherical	60nm	
GSE84982	CACO2	Spherical	20nm	
GSE84982	CACO2	Spherical	30nm	
GSE84982	CACO2	Spherical	60nm	
GSE20692	JURKAT	-	<100nm	
GSE84982	CACO2	Spherical	110nm	MYBPH WEE2 SULT2A1 FGA CENPA
GSE84982	CACO2	Spherical	20nm	
GSE84982	CACO2	Spherical	30nm	
GSE84982	CACO2	Spherical	60nm	
GSE84982	CACO2	Spherical	110nm	OAT
GSE84982	CACO2	Spherical	20nm	
GSE62253	CACO2	Spherical	15-28nm	
GSE84982	CACO2	Spherical	30nm	
GSE62253	CACO2	Spherical	15-28nm	HIST1H2AC
GSE20692	JURKAT	-	<100nm	
GSE84982	MCF7	Spherical	20nm	
GSE84982	MCF7	Spherical	30nm	
GSE84982	MCF7	Spherical	110nm	AFAP1L2
GSE84982	MCF7	Spherical	20nm	
GSE84982	MCF7	Spherical	30nm	
GSE84982	CACO2	Spherical	110nm	FGG FGB
GSE84982	CACO2	Spherical	20nm	
GSE84982	CACO2	Spherical	30nm	
GSE84982	MCF7	Spherical	20nm	PTPN6
GSE84982	MCF7	Spherical	30nm	
GSE84982	MCF7	Spherical	60nm	
GSE20692	JURKAT	-	<100nm	HIST1H3H HIST2H2AA3 ADCY1
GSE84982	MCF7	Spherical	20nm	
GSE84982	MCF7	Spherical	30nm	
GSE84982	CACO2	Spherical	110nm	KIF20A ANXA9
GSE84982	MCF7	Spherical	20nm	
GSE84982	MCF7	Spherical	30nm	
GSE84982	CACO2	Spherical	110nm	H1F0
GSE84982	CACO2	Spherical	20nm	
GSE20692	JURKAT	-	<100nm	
GSE84982	CACO2	Spherical	110nm	RBP2
GSE84982	CACO2	Spherical	20nm	
GSE62253	CACO2	Spherical	15-28nm	
GSE84982	CACO2	Spherical	110nm	REEP6 AMACR
GSE84982	CACO2	Spherical	30nm	
GSE84982	MCF7	Spherical	20nm	HIST3H2A RLN2 WISP2 AGR3

GSE84982	MCF7	Spherical	30nm	SOX3 SGK1 SCUBE2 SFXN2
GSE84982	CACO2	Spherical	110nm	MPC2
GSE84982	MCF7	Spherical	30nm	
GSE62253	CACO2	Spherical	15-28nm	MCEE
GSE84982	MCF7	Spherical	20nm	
GSE62253	CACO2	Spherical	15-28nm	HIST1H1C
GSE20692	JURKAT	?	<100nm	
GSE84982	CACO2	Spherical	110nm	CEBPD DIO1
GSE84982	CACO2	Spherical	20nm	
GSE84982	CACO2	Spherical	110nm	CDC25B FAM174B
GSE84982	CACO2	Spherical	60nm	
GSE62253	CACO2	Spherical	15-28nm	SPTLC3
GSE84982	CACO2	Spherical	60nm	
GSE84982	CACO2	Spherical	110nm	ICAM4 PRR15L ANG AGT
GSE62253	CACO2	Spherical	15-28nm	

Titanium

Dataset	Cell type	Morphology	Size	Downregulated shared genes
GSE42066	CACO2	Nanobelts	7x0,2x001nm	FCGR2A
GSE39316	HMDM	Spherical	27,4-35,2nm	
GSE42066	CACO2	Nanobelts	7x0,2x001nm	PHLDA1
GSE42067	SAE	Nanobelts	7x0,2x001nm	
GSE42066	CACO2	Nanobelts	7x0,2x001nm	CD44
GSE42068	THP1	Nanobelts	7x0,2x001nm	
GSE39316	HMDM	Spherical	27,4-35,2nm	TMEM187
GSE39316	JURKAT	Spherical	27,4-35,2nm	
GSE39316	HMDM	Spherical	27,4-35,2nm	NRP1 PAPPA2
GSE42067	SAE	Nanobelts	7x0,2x001nm	
GSE39316	JURKAT	Spherical	27,4-35,2nm	ZCCHC2
GSE42068	THP1	Nanobelts	7x0,2x001nm	
GSE42067	SAE	Nanobelts	7x0,2x001nm	TIPARP CCL2
GSE42068	THP1	Nanobelts	7x0,2x001nm	

Dataset	Cell type	Morphology	Size	Upregulated shared genes
GSE39316	MDDC	Spherical	27,4-35,2nm	AKAP13
GSE42068	THP1	Nanobelts	7x0,2x001nm	
GSE39316	JURKAT	Spherical	27,4-35,2nm	ENAH
GSE42068	THP1	Nanobelts	7x0,2x001nm	
GSE39316	HMDM	Spherical	27,4-35,2nm	SORL1
GSE42068	THP1	Nanobelts	7x0,2x001nm	
GSE42066	CACO2	Nanobelts	7x0,2x001nm	TTC3P1///TTC3 TCF25
GSE42068	THP1	Nanobelts	7x0,2x001nm	MED13L KIAA1033 ZNF148
GSE39316	MDDC	Spherical	27,4-35,2nm	DIS3
GSE42067	SAE	Nanobelts	7x0,2x001nm	
GSE42066	CACO2	Nanobelts	7x0,2x001nm	USP14
GSE39316	JURKAT	Spherical	27,4-35,2nm	

zinc

Dataset	Cell type	Morphology	Size	Downregulated shared genes

GSE39316	HMDM	Spherical	13-16,4nm	EXOG MT1E MT1H
GSE39316	JURKAT	Spherical	13-16,4nm	
GSE39316	MDDC	Spherical	13-16,4nm	
GSE39316	HMDM	Spherical	13-16,4nm	SOCS2 RIMS3 GPR162
GSE39316	JURKAT	Spherical	13-16,4nm	ZNF362 GPAT4 RAPGEFL1
GSE39316	JURKAT	Spherical	13-16,4nm	MT1G ATP6V1G2 MT1F
GSE39316	MDDC	Spherical	13-16,4nm	AARS2 MAPK1 ASB10 MT1A

Dataset	**Cell type**	**Morphology**	**Size**	**Upregulated shared genes**
GSE39316	HMDM	Spherical	13-16,4nm	MED8
GSE39316	JURKAT	Spherical	13-16,4nm	
GSE39316	MDDC	Spherical	13-16,4nm	
GSE39316	HMDM	Spherical	13-16,4nm	NCF4 NME6 GAS6 C21orf33
GSE39316	MDDC	Spherical	13-16,4nm	
GSE39316	HMDM	Spherical	13-16,4nm	NUDT1 ADSL
GSE39316	JURKAT	Spherical	13-16,4nm	
GSE39316	JURKAT	Spherical	13-16,4nm	KCNRG
GSE39316	MDDC	Spherical	13-16,4nm	

Suplemmentary Table 3

Suplemmentary Table 3: List of downregulated and upregulated pathways identified by Enrichr analysis.

Carbon				
Dataset	**Cell type**	**Morphology**	**Size**	**Downregulated Pathways**
GSE3364	HUVEC	Spherical	4,7-9,5nm	Terpenoid backbone biosynthesis
GSE43516	16LU	Spherical	Not reported	Ribosome Bacterial invasion of epithelial cells
GSE43515	16LU	Nanotube	Not reported	p53 signaling pathway Melanoma Glioma
GSE42068	THP1	Nanotube	5-10x20-30nm	TNF signaling pathway NF-kappa B signaling pathway Chemokine signaling pathway Cell cycle Cytokine-cytokine receptor interaction NOD-like receptor signaling pathway Malaria Epstein-Barr virus infection Toll-like receptor signaling pathway Folate biosynthesis Rheumatoid arthritis IL-17 signaling pathway AGE-RAGE signaling pathway in diabetic complications Shigellosis Epithelial cell signaling in Helicobacter pylori infection Cellular senescence Human T-cell leukemia virus 1 infection Influenza A Salmonella infection Transcriptional misregulation in cancer Kaposi sarcoma-associated herpesvirus infection Fluid shear stress and atherosclerosis Progesterone-mediated oocyte maturation

				Viral myocarditis p53 signaling pathway DNA replication Purine metabolism Homologous recombination
Dataset	**Cell type**	**Morphology**	**Size**	**Upregulated Pathways**
GSE43515	16LU	Spherical	Not reported	Protein processing in endoplasmic reticulum Amino sugar and nucleotide sugar metabolism
GSE43515	16LU	Nanotube	Not reported	Adherens junction MAPK signaling pathway Pathways in cancer Tight junction Rap1 signaling pathway Fc gamma R-mediated phagocytosis Endocytosis Shigellosis Pancreatic cancer Regulation of actin cytoskeleton Proteoglycans in cancer
			Silver	
Dataset	**Cell type**	**Morphology**	**Size**	**Downregulated Pathways**
GSE84982	CACO2	Spherical	110nm	Mineral absorption Ferroptosis Protein processing in endoplasmic reticulum IL-17 signaling pathway Fluid shear stress and atherosclerosis Galactose metabolism Pathways in cancer MAPK signaling pathway Osteoclast differentiation Colorectal cancer Estrogen signaling pathway Rheumatoid arthritis

GSE84982	CACO2	Spherical	110nm	Breast cancer Legionellosis Glutathione metabolism Central carbon metabolism in cancer Influenza A Epithelial cell signaling in Helicobacter pylori infection Fructose and mannose metabolism Pancreatic cancer Antigen processing and presentation Thyroid cancer Measles Salmonella infection
GSE84982	MCF7	Spherical	110nm	Mineral absorption Ferroptosis Glutathione metabolism Fluid shear stress and atherosclerosis
				Mineral absorption MAPK signaling pathway Pathways in cancer Breast cancer Colorectal cancer Thyroid cancer Ferroptosis Fluid shear stress and atherosclerosis p53 signaling pathway Salmonella infection Legionellosis Protein processing in endoplasmic reticulum Galactose metabolism Hepatocellular carcinoma Endometrial cancer Rheumatoid arthritis IL-17 signaling pathway Basal cell carcinoma

GSE84982	CACO2	Spherical	60nm	Estrogen signaling pathway Melanoma Pancreatic cancer Cellular senescence Cell cycle Human T-cell leukemia virus 1 infection Influenza A Osteoclast differentiation FoxO signaling pathway Small cell lung cancer Glutathione metabolism Kaposi sarcoma-associated herpesvirus infection Measles Apoptosis Steroid hormone biosynthesis Gastric cancer Epstein-Barr virus infection Central carbon metabolism in cancer Mitophagy Parathyroid hormone synthesis, secretion and action Non-small cell lung cancer Fructose and mannose metabolism Glioma Chronic myeloid leukemia Antigen processing and presentation
GSE84982	MCF7	Spherical	60nm	Hepatocellular carcinoma Mineral absorption Fluid shear stress and atherosclerosis Ferroptosis Pentose phosphate pathway Glutathione metabolism
				Mineral absorption MAPK signaling pathway Pathways in cancer

GSE84982	CACO2	Spherical	30nm	Protein processing in endoplasmic reticulum Apoptosis Colorectal cancer Thyroid cancer Ferroptosis Fluid shear stress and atherosclerosis Breast cancer Legionellosis Galactose metabolism Hepatocellular carcinoma Endometrial cancer Rheumatoid arthritis Influenza A Fructose and mannose metabolism IL-17 signaling pathway Small cell lung cancer Basal cell carcinoma Estrogen signaling pathway Melanoma p53 signaling pathway Pancreatic cancer Toxoplasmosis Antigen processing and presentation Human T-cell leukemia virus 1 infection Osteoclast differentiation Salmonella infection Glutathione metabolism Kaposi sarcoma-associated herpesvirus infection Transcriptional misregulation in cancer AGE-RAGE signaling pathway in diabetic complications HIF-1 signaling pathway Gastric cancer Phagosome Central carbon metabolism in cancer

				Mitophagy Parathyroid hormone synthesis, secretion and action Non-small cell lung cancer Epithelial cell signaling in Helicobacter pylori infection Cellular senescence Necroptosis Glioma Chronic myeloid leukemia
GSE84982	MCF7	Spherical	30nm	Mineral absorption Fluid shear stress and atherosclerosis Ferroptosis Glutathione metabolism
GSE84982	CACO2	Spherical	20nm	Mineral absorption MAPK signaling pathway Pathways in cancer Colorectal cancer Thyroid cancer Protein processing in endoplasmic reticulum Ferroptosis p53 signaling pathway Apoptosis Breast cancer Legionellosis Endometrial cancer IL-17 signaling pathway Estrogen signaling pathway Basal cell carcinoma Fluid shear stress and atherosclerosis Melanoma Pancreatic cancer Cellular senescence Hepatocellular carcinoma Human T-cell leukemia virus 1 infection Influenza A

				Osteoclast differentiation Small cell lung cancer Measles AGE-RAGE signaling pathway in diabetic complications Gastric cancer Galactose metabolism Parathyroid hormone synthesis, secretion and action Central carbon metabolism in cancer Non-small cell lung cancer Glioma Chronic myeloid leukemia Antigen processing and presentation Cell cycle
GSE84982	MCF7	Spherical	20nm	Mineral absorption Ferroptosis Glutathione metabolism Protein processing in endoplasmic reticulum Hepatocellular carcinoma Antigen processing and presentation Fluid shear stress and atherosclerosis Legionellosis Steroid hormone biosynthesis Arachidonic acid metabolism Pentose phosphate pathway
GSE62253	CACO2	Spherical	15-28nm	Mineral absorption MAPK signaling pathway Protein processing in endoplasmic reticulum Ferroptosis Rheumatoid arthritis IL-17 signaling pathway Legionellosis Influenza A Spliceosome Estrogen signaling pathway

				Measles
GSE14452	HEPG2	Not reported	7-10nm	Cell cycle DNA replication Pyrimidine metabolism Epstein-Barr virus infection Mismatch repair Human T-cell leukemia virus 1 infection Proteasome Nucleotide excision repair Homologous recombination Cellular senescence Alzheimer disease
GSE20692	JURKAT	Spherical	<100nm	Mineral absorption Alanine, aspartate and glutamate metabolism Progesterone-mediated oocyte maturation Vitamin B6 metabolism Oocyte meiosis

Dataset	Cell type	Morphology	Size	Upregulated Pathways
GSE84982	CACO2	Spherical	30nm	Complement and coagulation cascades Platelet activation
GSE84982	MCF7	Spherical	30nm	Systemic lupus erythematosus Alcoholism Viral carcinogenesis Estrogen signaling pathway Necroptosis
GSE84982	CACO2	Spherical	20nm	Complement and coagulation cascades Platelet activation
GSE84982	MCF7	Spherical	20nm	Systemic lupus erythematosus Alcoholism Estrogen signaling pathway Viral carcinogenesis Proteoglycans in cancer
				Hematopoietic cell lineage

				Thyroid hormone synthesis Systemic lupus erythematosus Non-homologous end-joining Alcoholism Vascular smooth muscle contraction Insulin secretion GnRH signaling pathway Cellular senescence Human cytomegalovirus infection Parathyroid hormone synthesis, secretion and action cGMP-PKG signaling pathway
GSE20692	JURKAT	Spherical	<100nm	Cholinergic synapse Cortisol synthesis and secretion Long-term potentiation Calcium signaling pathway Gap junction Cushing syndrome Aldosterone synthesis and secretion Pancreatic secretion Inflammatory mediator regulation of TRP channels Protein processing in endoplasmic reticulum Chagas disease (American trypanosomiasis) Amyotrophic lateral sclerosis (ALS) Th17 cell differentiation

Titanium

Dataset	Cell type	Morphology	Size	Downregulated Pathways
GSE42067	SAE	Nanobelts	7x0,2x001nm	AGE-RAGE signaling pathway in diabetic complications Cytokine-cytokine receptor interaction TNF signaling pathway Cytokine-cytokine receptor interaction Rheumatoid arthritis NF-kappa B signaling pathway IL-17 signaling pathway

GSE42068	THP1	Nanobelts	7x0,2x001nm	Chemokine signaling pathway NOD-like receptor signaling pathway Transcriptional misregulation in cancer Malaria Salmonella infection Epithelial cell signaling in Helicobacter pylori infection Kaposi sarcoma-associated herpesvirus infection Pathways in cancer Small cell lung cancer Legionellosis Viral myocarditis Shigellosis Epstein-Barr virus infection Fluid shear stress and atherosclerosis Human T-cell leukemia virus 1 infection Phospholipase D signaling pathway Human cytomegalovirus infection Ras signaling pathway Necroptosis Intestinal immune network for IgA production Toll-like receptor signaling pathway C-type lectin receptor signaling pathway VEGF signaling pathway Rap1 signaling pathway

Dataset	Cell type	Morphology	Size	Upregulated Pathways
GSE42066	CACO2	Nanobelts	7x0,2x001nm	Parathyroid hormone synthesis, secretion and action Proteoglycans in cancer Choline metabolism in cancer Non-small cell lung cancer PI3K-Akt signaling pathway Bladder cancer
GSE42067	SAE	Nanobelts	7x0,2x001nm	Cell cycle
GSE42068	THP1	Nanobelts	7x0,2x001nm	Platelet activation

Zinc				
Dataset	**Cell type**	**Morphology**	**Size**	**Downregulated Pathways**
GSE39316	HMDM	Spherical	13-16,4nm	Ferroptosis
GSE39316	JURKAT	Spherical	13-16,4nm	Mineral absorption
GSE39316	MDDC	Spherical	13-16,4nm	Mineral absorption
Dataset	**Cell type**	**Morphology**	**Size**	**Upregulated Pathways**
GSE39316	HMDM	Spherical	13-16,4nm	Allograft rejection Graft-versus-host disease Type I diabetes mellitus Antigen processing and presentation Autoimmune thyroid disease Viral myocarditis Phagosome Human T-cell leukemia virus 1 infection Cell adhesion molecules (CAMs) Viral carcinogenesis Epstein-Barr virus infection